Theoretical and Experimental Investigation of the Acoustic Behavior of Visco-Elastically Damped Cylindrical Shells

Michael Klausbruckner

Dipl.Ing. Fachhochschule Munich (1990)
M.S. Worcester Polytechnic Institute (1992)

Submitted in Partial Fulfillment of the Requirements for the Degree of

Master of Science

at the

Massachusetts Institute of Technology

August 1995

Signature of Author _____
Department of Ocean Engineering
August of 1995

Certified by _____
Assistant Professor J. Robert Fricke
Thesis Supervisor

Accepted by _____
Professor A. Douglas Carmichael
Chairman, Department Graduate Committee

Theoretical and Experimental Investigation of the Acoustic Behavior of Visco-Elastically Damped Cylindrical Shells

by Michael J. Klausbruckner

Submitted to the Department of Ocean Engineering in partial fulfillment
of the requirements for the Degree of Master of Science in Ocean Engineering

Abstract

This thesis investigates the mid-frequency scattering from fluid-loaded, visco-elastically damped cylindrical shells. Previous studies have examined the acoustic backscatter from empty and internally-loaded shells with no damping treatment, demonstrating the primary importance of shear waves traveling along a helical path on the shell. As a result, a theoretical and experimental analysis was conducted studying the influence of a constrained layer on the back scattering behavior of a visco-elastically damped shell subjected to fluid loading on the outside. As the experimentally generated scatter is very complex, theoretical models were used to identify and isolate acoustic and elastic wave processes present during and after insonification. The theoretical analysis, centered on a thin-shell model, describes the acoustics of an infinitely long cylindrical shell used to assess the overall loss-factor of the constrained layer shell. Experimental results are based on the analysis of monostatic and bistatic measurements conducted over the mid-frequency range ($2 < ka < 10$) corresponding to 3/4 to 3 times the ring frequency of the shell. The analysis of the experimental data demonstrates that the constrained layer effectively attenuates helical shear waves, thereby reducing their radiation into the fluid. Therefore, the direct acoustic scattering pattern from impedance discontinuities is more prominent in the case of the damped shell. Thus, in contrast to the undamped shell, the damped shell shows a reduction of 3 - 5 dB in the integrated target strength for all angles of insonification ranging between 0 degrees and 90 degrees.

Thesis Supervisor: Dr. J. Robert Fricke
Title: Assistant Professor of Ocean Engineering, M.I.T.

Dedicated to Elley and my family

"Achievement comes from strength, but
strength is drawn from family."

Acknowledgments

A thesis is not the work of an individuum, but the product of many: mentors, colleges, and family. I would like to thank my mentor and advisor, Professor J. Robert Fricke, who not only brought me 'aboard', but also encouraged and supported me in all my endeavors at MIT. You always found the time to discuss academic issues. However, you taught me much more than only academic wisdom and I enjoyed our conversations on travels and during invitations to your home. I wish you the best in securing a tenure position at MIT.

If it was not for Professor Ira Dyer's financial and academic support, this research work would not have been possible. His vast knowledge about acoustics has been a fountain of wisdom to me. His 'unconventional' approach of modeling complex acoustical processes separately and simplifying each process to its essentials proved to be invaluable in my research work.

Yueping Guo, I wish you the best at your new occupation! Many times I came to you and asked you for advice, and you always made the time to explain acoustic methods to me and provided me with invaluable suggestions. I am a little bit sad, that you left the academic world, because you belong to the best teachers I ever met. But maybe - one day you will be a teacher again and will share with us your outstanding engineering knowledge and expertise.

I certainly will not forget my office-colleges Joe Bondaryk ('Dr. Joe'), Matthew Conti ('Matti'), Peter Daly ('Mr. Linux'), Tarun Kishore Kapoor ('Tikka'), Vincent Hugh Lupien ('Hugh, Lups'), Jeongho Park ('Mr. Pak'), and Brian Sperry ('The Sperryman'). You guys made my stay at MIT a real pleasure! Your humor kept me 'alive' through long and busy days in the office. Especially Tarun's funny and skillful play with words made me laugh countless times. It's no secret that 'Dr. Joe' has a big comedy talent and his fame reaches far beyond our office; I had an excellent time to witness your persiflage on "famous individuals".

There are many more, who will be remembered. One will be Sabina Rataj, whose humor and experience helped me out many times. Your parties were excellent Sabina! At this point I also want to include the always happy Isella Cordova and Taci Darnell in my acknowledgments.

Last but not least I want to thank my fiancé for her love and emotional support, which had to reach me over 4000 Miles across the US-continent. I promise, one day we will be united again and I am looking forward to that day ...

Table of Contents

List of Figures

List of Tables

Chapter 1

Introduction

In the following the motivation and practical relevance for the research on visco-elastically damped cylindrical shells is demonstrated. Results of previous research on the acoustical and vibrational behavior of cylindrical shells are briefly summarized and references for further study are given.

1.1. Research Motivation

Cylindrical shells have many industrial applications - they serve as storage containers, protection systems against external or internal influences (i.e., cylindrical pressure vessels), or allow for convenient transportation of liquid and gaseous media (pipelines). Further - by utilizing their structural stability for underwater vehicles - they also provide means to explore our oceans and in this way help us to understand a quite different world than the one to which we are accustomed. Especially in the design of submarines, the approximation of the hull with a cylindrical shell and subsequent analyses based on this geometrical simplification have proved to be very useful.

Cylindrical shells, or for that matter submarine hulls, are subjected to a variety of external influences and parametric optimization of the shell design requires an understanding of the shell behavior under specific external influence. One of the external influences to which a shell can be subjected is a sound wave interacting with the exterior surface and

causing elastic deformations of the shell. These time-varying, elastic deformations induce a sound field, which radiates into the surrounding fluid and is superimposed onto the original sound field. This observation, that the pressure field is dominated not only by the directly reflected (scattered) wave, but also by membrane waves acoustically excited and emanating from the shell surface, was experimentally verified by an analysis of measurement data of fluid-loaded, undamped shells under sound wave excitation [1]. The analysis of the results of these experiments on fluid-loaded, undamped shells raised the following questions:

- Can membrane waves be efficiently attenuated?
- How should parameters governing the acoustic behavior in the new shell design be chosen to minimize sound radiation from the shell?

A literature search revealed that, in the past, the acoustical analysis of the acoustic scattering behavior of fluid-loaded circular shells has been limited to non-dissipative shell designs in the mid-frequency range (see Section 1.2. Results of Previous Research of Acoustic Analysis on Shells; it should be noted that the research on one-sided coated shells is focused on the high frequency response of the shell and therefore will not be mentioned any further). As a consequence no answers could be found to the posed questions.

In search for an effective shell design for attenuating membrane waves, it is recalled from experience, that the application of a visco-elastic layer in a sandwich design is known to produce high attenuation in plates - especially for flexural waves [12]. However, the pressure field induced by flexural waves for fluid loaded structures is exponentially decaying away from the shell in the frequency range of interest, and therefore any scattering pattern observed in the far field will not be dominated by the effect of this wave type. Shear and compressional waves, which are supersonic with respect to the speed of sound in water, will be observable in the far-field of the shell. Even though the physics of supersonic waves are quite

different to the physics of flexural waves, it seemed worthwhile to study the application of a constrained-layer sandwich design for cylindrical shells and the attenuation of supersonic membrane waves.

To study the attenuation effect of a visco-elastic layer, a theoretical model was developed; it describes the acoustic behavior of a sandwich design for cylindrical shells. The model was used to roughly quantify the amount of attenuation achievable by a sandwich shell design. It is noted that the results of this model are based on fluid-loaded empty shells, but in general, shells will be loaded with internal structures, which are coupled to the shell and this, in turn, will affect the scattering behavior of the shell. A physical experiment was needed to answer the question of how close the prediction of attenuation for a damped empty shell matches a 'real-life scenario' and also to answer how internal loading affects the attenuation of a damped, fluid loaded shell. Therefore, a model was designed and tested; the model incorporates a three-layer sandwich shell and internal loadings to study the attenuation of supersonic waves in the mid-frequency range from ka = 2 to ka = 10. A plane wave was used to excite the fluid loaded model under consideration for various orientation angles of the shell with respect to the plane wave front. Then data from monostatic and bistatic measurements were signal processed and analyzed to study the acoustic backscatter from the shell.

1.2. Results of Previous Research on Acoustic Analysis on Shells

There has not been a great deal of research work in the analysis of damped shells in the mid-frequency range [1,7,8]. The cited work on damped shells is of theoretical nature and no reported experiments have been performed to verify these theoretical results. As a consequence,

emphasis will be placed on theoretical methods and their results in the discussion of previous research on damped shells. Since the physics of damped and undamped shells are similar, an understanding of the undamped shell behavior provides the necessary knowledge to model and to interpret the damped shell behavior. It will prove helpful to take a closer look at results from undamped shells before the analysis results of previous research on damped shells is discussed.

In general the backscattering behavior of a cylindrical shell is determined by its acoustical and structural properties: it was shown previously [1], that the total, experimentally measured shell response can be synthesized from 1) an elastic and 2) a purely geometric shell return. To be more precise, an initial sound wave is reflected from the cylinder as well as exciting waves on the cylinder surface. From an acoustical point of view it is obvious that the waves on the cylinder are influenced by the structure's acoustical properties. In contrast, the directly-reflected return is not influenced (in a first approximation) by the acoustical properties of the shell in the mid-frequency range, and it can be assumed to be widely unaffected by the elastic response of the shell. Therefore the interest lies in the analysis of waves which are excited on the shell surface.

As mentioned before, most of the work in the acoustical analysis of cylindrical shells has concentrated on the theoretical aspect of the study of the shell behavior. Various theoretical models [1-8] describing the shell deformations under acoustic excitation have been proposed. In general the cylinder under consideration is thin-walled, i.e., its thickness to radius ratio is about 1% to 3%, where this value for the shell thickness leads to the characterization of these waves as membrane waves. Therefore all the models consider a first-order approximation of the strains in deriving the equations of motion, but they differ in the solution approach of the governing differential equations. In characterizing the effect of these waves, it is customary to use either a

modal approach or a wave approach. It can be shown that both methods are mathematically equivalent. However, it is noted, that the modal approach - though providing a powerful method in low frequency analysis in general - is cumbersome to apply for high frequencies, mainly because then the structural response is based on a high modal density, which makes a simple physical characterization of the structure difficult [2]. As a result, for high frequencies a great deal of research work has centered on a simplifying analysis of cylindrical shells by applying ray concepts [3-7]. In addition, solution functions were constructed which incorporate both concepts [1,8]. The advantage in the mid/high-frequency analysis of using a ray method is based on the fact, that the effect of a "sound field" can be represented by individual effects of so-called "sound rays", which then allows the investigator to consider only one ray at a time. Further it is noted, that there is no "physical" disadvantage to the well-known modal approach, because modes can be synthesized from rays by combining them, which demonstrates the equivalence of these two methods. However, as mentioned above an analysis based on modes is cumbersome in the mid-frequency range due to the high modal density of the shell. In studying the interaction of the sound wave with the cylinder as it travels along its path, it is only necessary to consider the local effect of the structure on the ray behavior and vice versa. Then the effect of the total sound field can be obtained by combining the effects of the individual ray contributions.

The simplification in the acoustical analysis by using a ray concept lead to a very intuitive understanding of experimental data on backscattering from cylindrical shells. Norris and Rebinsky [3], as well as Pierce and Kil [6], demonstrated that the prevailing wave types can be grouped into membrane waves, longitudinal and shear, and flexural waves. By using short wave length asymptotics, Norris et al.[3] were able to define the direction of polarization for each wave type. In other words, the polarization of the wave or the function of propagation direction is greatest along a specific path for each wave type. Longitudinal waves have polarizations that

cluster near the principal direction of greatest curvature and less for the other direction. Shear waves are polarized in directions away from the principal curvatures, which in the case of a cylindrical shell will result in a helical path of propagation. The latter result was confirmed also through several other investigations [1,2].

It is an interesting, though not surprising, fact that the ray paths coincide with the geodesic of the shell if the wave speed is constant, but can depart from these, if the wave speed varies with position [4]. With respect to this finding, Norris was able to show for the thin-shell approximation that the shear and longitudinal wave speeds are constant even if the shell thickness is variable (however, flexural wave speeds will change with variable shell thickness). As the membrane waves, such as shear and compressional waves, travel on the shell surface they excite a field in the surrounding fluid. Whether this acoustic field is propagating freely or evanescent is dependent on the ratio of the wave speed on the shell to the wave speed in the fluid. In this study a water loaded metallic shell is considered, which ensures that membrane waves are supersonic and will produce a freely propagating acoustic field. Rays, which have interacted with the elastic medium are launched from the shell into the surrounding fluid (water). Corrado [1] and Norris et al. [5] have studied the launch conditions under which, so called leaky waves, will radiate into the fluid. In the case of an infinite cylinder both research works could prove that the launch line of leaky waves is an infinite straight line parallel to the cylinder axis. In addition, they showed coupling of the shell field to the fluid is possible, only if the incidence angle is less than the critical angle. It is expected, that this observation is also true for damped shells, but the wavespeeds on damped shells might be different from wavespeeds on undamped shells.

Chapter 2

Theoretical Model and Results

In this section a theoretical model for visco-elastically damped cylindrical shells is developed in order to quantify the attenuation of elastic waves. The results of this model are compared to the results of a model based on the full-elastic theory [8] generally known to be computationally expensive, but to produce very accurate results.

The results of these two analytical models are used to assess and to quantify the attenuation of supersonic waves for various aspect angles, as well as to explain differences in the scattering levels between the untreated and the damped shell due to different shell thicknesses. Neither of these models consider internal loadings, and even though the internals do affect the overall attenuation levels, to a first approximation the results of the empty shell models can be used to roughly quantify the damping effect of a shell with internal complexity (as it was experimentally verified [1]).

The analytical model developed here is based on the classical thin-shell theory and provides a simple correlation for estimating an overall loss factor for the shell, where the overall effective loss factor [7] is expressed as a weighted average of the individual loss factors of the shell layers.

Corrado [1] found in his theoretical and experimental analysis of shells, that the results based on thin-shell theory for fluid-loaded, isotropic shells compare well with experimental results for the employed shell parameters. Therefore it was expected *a priori*, that the modified thin-shell model would compare well with experimental results of an empty damped shell. This will be the case, as long as the model is valid, meaning that the assumptions made about the shell behavior are not violated, see Appendix A1-1. Before experiments were conducted, the validity of the thin-

shell theory in the analysis of scattering from visco-elastically damped shells was determined by utilizing the results of a more general full-elastic model for multilayered shells developed by Ricks [8]. However, the advantage of using a thin-shell model over a full-elastic model is to consider quickly the essential parameters governing the acoustic scattering problem of cylinders. This approach provides a simplified and more intuitive understanding of the elastic shell response.

2.1. The Thin-Shell Model

It is known, that the interface of a shell with a relatively heavy fluid medium presents a strongly coupled interactive system. The dynamic response differs considerably from that of an isolated structure in vacuo. Thus, the forced acoustical response of a three-layer sandwich cylindrical shell with induced fluid loading is formulated as the basis for determining the damping effect of a visco-elastic layer upon the fluid-structure response.

The considered shell structure consists of three isotropic layers with different thicknesses. Two cylindrical elastic shells are bonded together with a visco-elastic core material to form a composite structure of mean radius a. The overall shell thickness is considered to be small in comparison with the other dimensions of the shell and with its radius of curvature. It is assumed that the three layers are joined together by a perfect bond, which enforces the continuity of displacement at the interfaces. The material of the face layers is Nickel and the core material is a visco-elastic material, where tangential shear deformation is taken into account. The equations of motion for the visco-elastically damped shell are derived on the basis of D'Alemberts Principle (see Appendix A.1-1). To evaluate the internal forces, an infinitesimal element is formed by two pairs of adjacent planes which are normal to the surface of the shell. The coordinate axes, x and y, are tangent to the coordinate origin and the z-axis is normal to the middle surface. The axial,

circumferential, and radial displacement components u, v, w acting on an infinitesimal part of the shell and represented by their respective forces are shown in Figure 1.

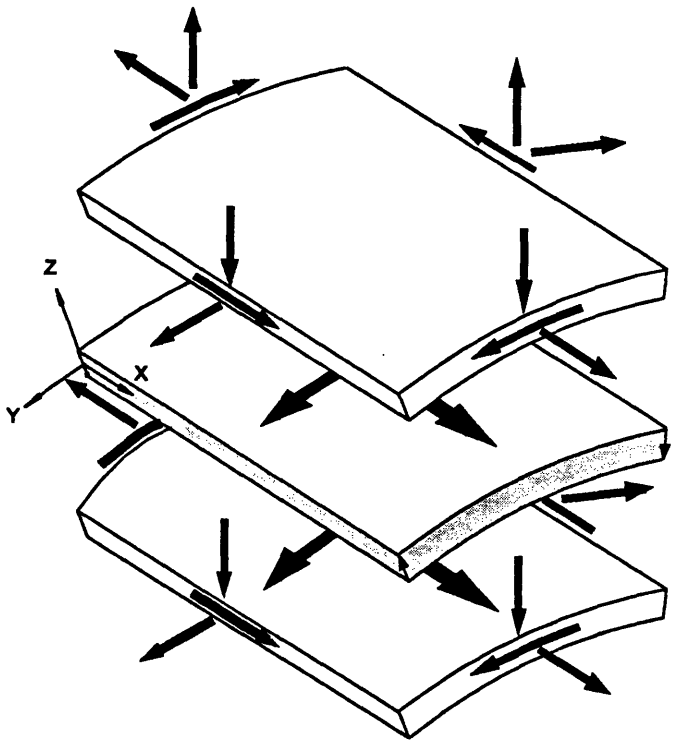

Figure 1. Coordinate system and force direction of an infinitesimal element of the visco-elastically damped shell.

If the mass of the visco-elastic material is low compared to the mass of the face layers, then the forces of the core-layer may be neglected, which will result in a 5x5 system matrix for the equation of motion (see Appendix A1-1 for detailed development of the governing equation of motion for a three-layered system). All the thin-shell results shown subsequently are based on the solution of Eq. (A.7).

Regarding the number of equations in the system matrix, note that all visco-elastic

materials are stiff in compression, and therefore, the radial displacement is assumed to be the same for all three layers. Guo [7] showed that the number of equations can be further reduced resulting in a set of equations which is similar to the Donnell-equations of motion. This reduced set of equations can be written as,

$$\frac{\delta^2 u}{\delta x^2} + \frac{1-\sigma}{2}\frac{\delta^2 u}{\delta \phi^2} + \frac{1+\sigma}{2}\frac{\delta^2 v}{\delta x \delta \phi} + \sigma\frac{\delta w}{\delta x} - \alpha_0\frac{\delta}{\delta x}\nabla^2 w = -\rho\varpi\frac{\delta^2 u}{\delta t^2}\,, \tag{1}$$

$$\frac{1+\sigma}{2}\frac{\delta^2 u}{\delta x \delta \phi} + \frac{1-\sigma}{2}\frac{\delta^2 v}{\delta x^2} + \frac{\delta^2 v}{\delta \phi^2} + \frac{\delta w}{\delta \phi} - \alpha_0\frac{\delta}{\delta \phi}\nabla^2 w = -\rho\varpi\frac{\delta^2 v}{\delta t^2}\,, \tag{2}$$

$$\gamma\frac{\delta u}{\delta x} + \frac{\delta v}{\delta \phi} + w + \beta\nabla^4 w - \alpha_0\nabla^2\left(\frac{\delta u}{\delta x} + \frac{\delta v}{\delta \phi}\right) - 2\alpha_0\frac{\delta^2 w}{\delta \phi^2} - 2\lambda\frac{\delta^2 w}{\delta x^2} = \varpi\left(\rho\frac{\delta^2 w}{\delta t^2} - p_i\right) \tag{3}$$

where

$$h = \sum_{j=1}^{N} h_j\,, \qquad \rho = \sum_{j=1}^{N} \rho_j h_j\,,$$

$$\varpi = \left(\sum_{j=1}^{N} \frac{E_j h_j}{1-\nu_j^2}\right)^{-1}, \qquad \alpha_0 = \varpi \sum_{j=1}^{N} \frac{E_j h_j (h_j + 2z_j)}{2(1-\nu_j^2)},$$

$$\sigma = \varpi \sum_{j=1}^{N} \frac{E_j h_j \nu_j}{1-\nu_j^2}, \qquad \lambda = \varpi \sum_{j=1}^{N} \frac{E_j h_j \nu_j (h_j + 2z_j)}{2(1-\nu_j^2)},$$

$$\beta = \varpi \sum_{j=1}^{N} \frac{E j h_j}{3(1-\nu_j^2)} (h_j^2 + 3h_j z_j + 3z_j^2)\,,$$

Here, ∇^2 is the Laplacian differential operator in cylindrical coordinates, $\nabla^4 = \nabla^2 * \nabla^2$, E_j represents the Youngs modulus for the *j*th layer *(j=1,3)*, and ρ_j denotes the shell density for each layer. Moreover, h_j and ν_j is the thickness and the Poisson ratio for each layer, respectively, and p_i denotes the incidence pressure. Further, z_j is introduced which quantifies the radial offset of the lower bounding surface of the *j*th layer. Clearly, this form of representation of the governing

equation of motion, Eqs (1) to (3), is more compact than the set of equation in Eq. (A.7). The above set of equations is shown only to highlight the similarity between the multi-layer model and the single-layer (Donnell) model. Indeed this similarity should be no surprise, because the multi-layer models, as well as the single layer model, are based on the same first order (thin-shell) theory. However, equations (1) to (3) show this similarity more clearly than the equations in Eq. (A.7). On the other hand Eqs (A.7) demonstrate that only the face-layer forces are of primary importance in the acoustic modeling of the sandwich shell behavior and the influence of the core-layer may be neglected. Regardless whether all the forces, Eqs. (1) to (3), or only the face layer forces, Eq. (A.7) (see Appendix A1-1), are considered, the governing equations of motion will reduce to the single-layer Donnell-Mushtari shell equations, if the core layer thickness is assumed to be zero. Further, Eqs (1) to (3) show, that if the layers are symmetric around the middle layer, the parameters λ and α will vanish, and the newly obtained equations will represent the well known single-layer shell equations. Note, that all thin-shell results shown in the following figures were obtained from the 5x5 system matrix, shown in Eq. (A.7) of Appendix A1-1.

The loss factor of the face layers is assumed to be small as compared to the loss factor of the visco-elastic material, which is incorporated through a complex value of the Young's modulus, E_j (see also Appendix A1-3). Note, that typical values for face-layer loss-factors are two to three order of magnitudes smaller than that for the core-layer. Therefore the face-layer loss-factor may be neglected in the theoretical prediction of the shell response.

2.2. Solution of the Equation of Motion with Fluid-Loading

Solutions to the governing problem can be found, once a general mathematical relationship between the incident and the scattered pressure is determined.

The cylindrical shell is insonified by a plane wave at oblique angles of incidence. In

any case, the scattered field propagating away from the shell is governed by the simplified wave equation,

$$\nabla^2 p_s + k^2 p_s = 0 \ , \tag{4}$$

where p_s represents the scattered pressure. The scattered pressure field is influenced by the incidence plane wave field described by,

$$p_i = P_o \, e^{\,i \vec{k} \cdot \vec{x}} \ , \tag{5}$$

where P_o is the amplitude of the incidence pressure and $\vec{k}$ denotes the wavenumber vector. The coupling between the elastic shell response and the fluid medium is governed by the frequency domain momentum equation, applied at the shell radius,

$$\frac{\delta p_s}{\delta z} + \frac{\delta p_i}{\delta z} = k^2 w \ . \tag{6}$$

Based on the geometry of the object studied, it is convenient to express the incident pressure field by using cylindrical wave functions as (see Appendix A1-2)

$$p_i = P_o \, e^{ik_x x} \, \Sigma_{n=0}^{\infty} \, \epsilon_n \, i^n J_n(k_z z) \cos(n \phi) \ , \tag{7}$$

where k_x represents the axial wavenumber, n represents the circumferential mode number, $\epsilon_n = \begin{cases} 1 & (n = 0) \\ 2 & (n > 0) \end{cases}$, and J_n is the cylindrical Bessel function of the first kind. Then the scattering field can be described by,

$$p_s = P_o \, e^{ik_x x} \, \Sigma_{n=0}^{\infty} \, C_n \, \epsilon_n \, i^n H_n(k_z z) \cos(n \phi) \ , \tag{8}$$

where C_n is the scattering Fourier coefficient and H_n is the cylindrical Hankel function of the first kind, see Appendix A1-2.

The mathematical description of the scattered pressure is based on a modal approach in the circumferential direction and a 'traveling' wave approach in the axial direction. Note, that there is only one wavenumber in axial direction and therefore no integration over wavenumbers has to be carried out. The assumed solution function for the displacement components in the three coordinates are

$$
\begin{aligned}
u^{\alpha} &= e^{ik_x x} \Sigma_{n=0}^{\infty} U_n^{\alpha} \epsilon_n i^n \cos(n\phi) , \\
v^{\alpha} &= e^{ik_x x} \Sigma_{n=0}^{\infty} V_n^{\alpha} \epsilon_n i^n \sin(n\phi) , \\
w &= e^{ik_x x} \Sigma_{n=0}^{\infty} W_n \epsilon_n i^n \cos(n\phi) ,
\end{aligned}
\tag{9}
$$

where $i^n = (-1)^{n/2}$, and U_n^{α}, V_n^{α}, W_n represent the Fourier coefficients for the inner (α=i) and outer (α=o) layers, respectively (see Appendix A1-1).

Finally, solutions to the governing problem are obtained, if the differential system synthesized by the equations of motion, Eq.(A.7), and the momentum equation, Eq.(6), is transformed into an algebraic system by applying the transformations in Eqs.(7) to (9). The resulting (coupled) system of Fourier coefficients is solved numerically through matrix inversion.

2.3. Theoretical Results for Fluid-Loaded Cylindrical Shells

Figures 2 and 3 show a comparison between the results of the thin-shell theory (based on Eq. (A.7), Appendix A1-1) and the results of the full-elastic theory [8] for the two employed thickness ratios. The form functions in Figure 2 show the typical pressure distribution across frequencies for a cylindrical shell based on the results of the two different models. The minima of the form function are produced by destructive interference of the leaky wave field radiated off the shell and the specular reflected wave field. Higher frequencies show less pronounced minima, which are due to smaller values in the shell surface displacements during resonance.

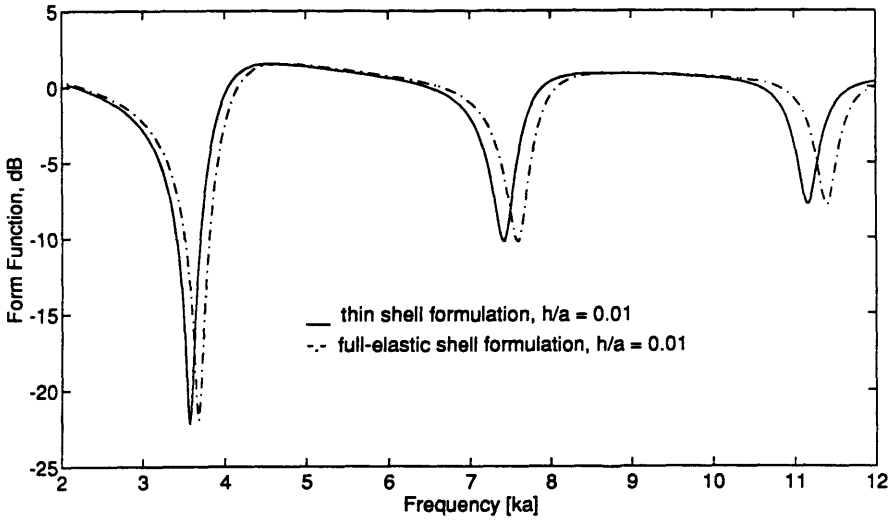

Figure 2. Comparison of the results obtained by thin-shell theory and full-elastic theory for a single-layer cylindrical shell, insonified with a plane wave at beam aspect.

In general, there is a good agreement between the result of the thin-shell theory and the results obtained by the full-elastic theory. The shape of the form function is very similar in both models, but the minima occur at slightly different frequencies.

At beam aspect, the deviations between back scattering pressure levels increase with frequency. Ricks [8] studied the differences between results obtained from his full-elastic model and results obtained from a single-layer thin-shell model. He pointed out, that there is an increase in deviation between the minima of the thin-shell and the full-elastic theory for increasing frequencies. This is confirmed in Figure 2. In the region between ka = 2 and ka = 10, the thin shell equations, Eq. (A.7), generate results for the scattering pressure, which compare very well with results obtained by the full-elastic theory.

Figure 3 shows a comparison between results of the thin-shell theory and the full-elastic theory for a shell with an increased thickness to radius ratio, where the value for this thickness to radius ratio represents the shell parameters of the experimentally tested composite shell.

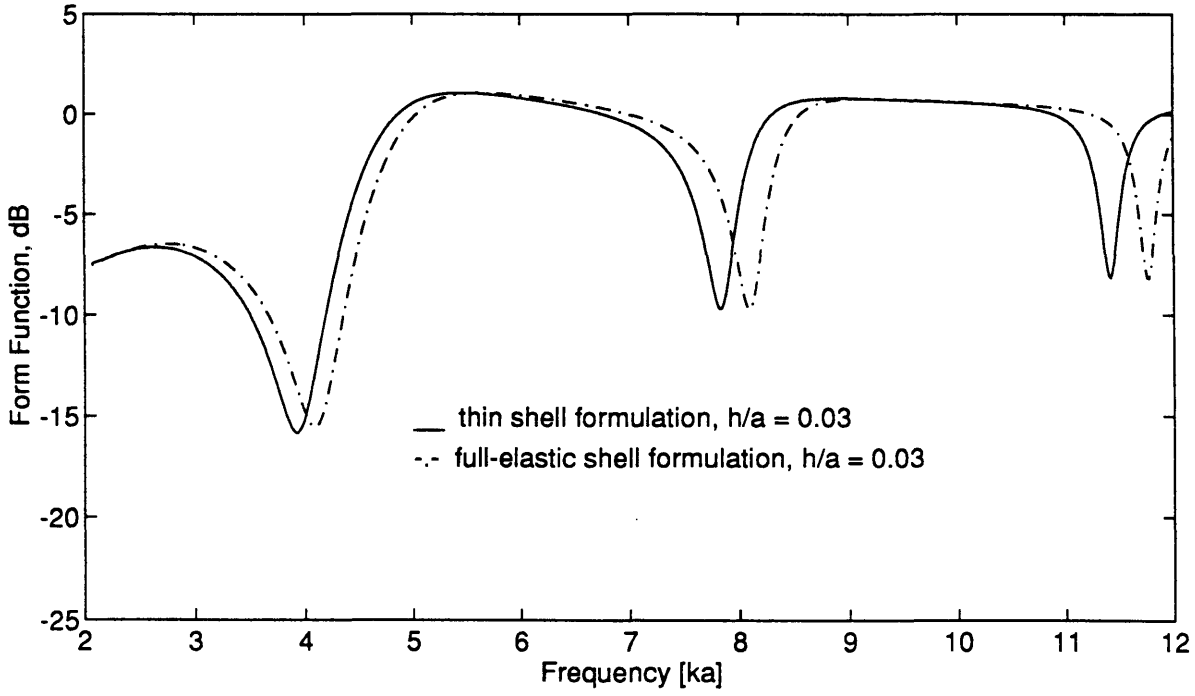

Figure 3. Comparison of the results between thin-shell and full-elastic theory, for insonification of a single layer shell with a plane wave at beam aspect and increased thickness to radius ratio.

Again, very good agreement between the results of the two employed models is obtained. If the shell is damped by a constrained visco-elastic layer, it will be expected, that the surface displacement of the shell during resonance will be reduced and as a consequence the minima, shown in Figure 2, will become shallower, see Figure 4. In addition, it is noted, that the maximum pressure levels are slightly decreased. The damping process can be demonstrated also in the time domain, as shown in Figure 5. As shown by Corrado [1], the "specular reflected field shows little variation with the addition of structural damping" while leaky wave levels show the expected decrease.

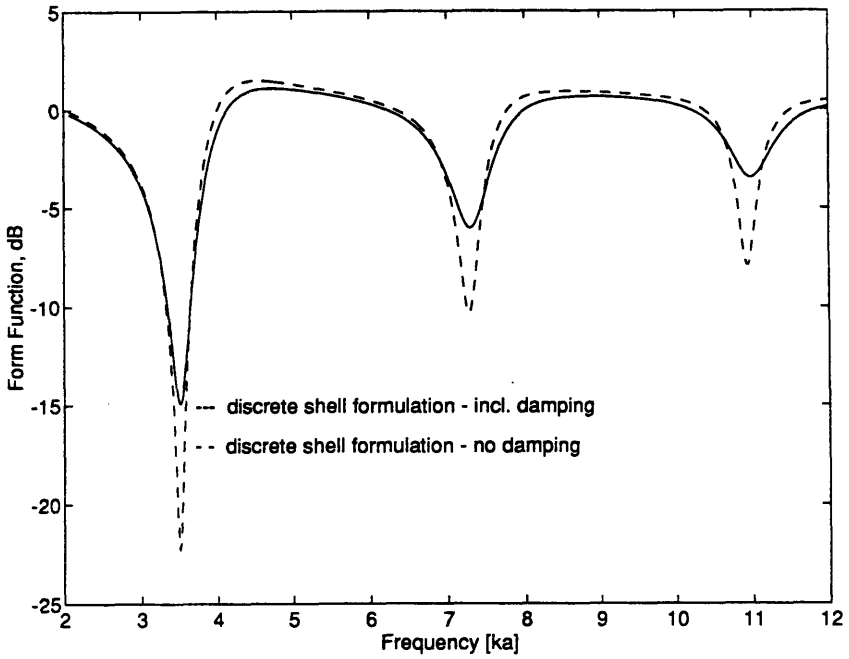

Figure 4. Back scattering form function of an undamped and damped cylindrical shell at normal incidence in the frequency domain. The loss factor of the visco-elastic layer of a damped shell with equal layer thickness is assumed to be one.

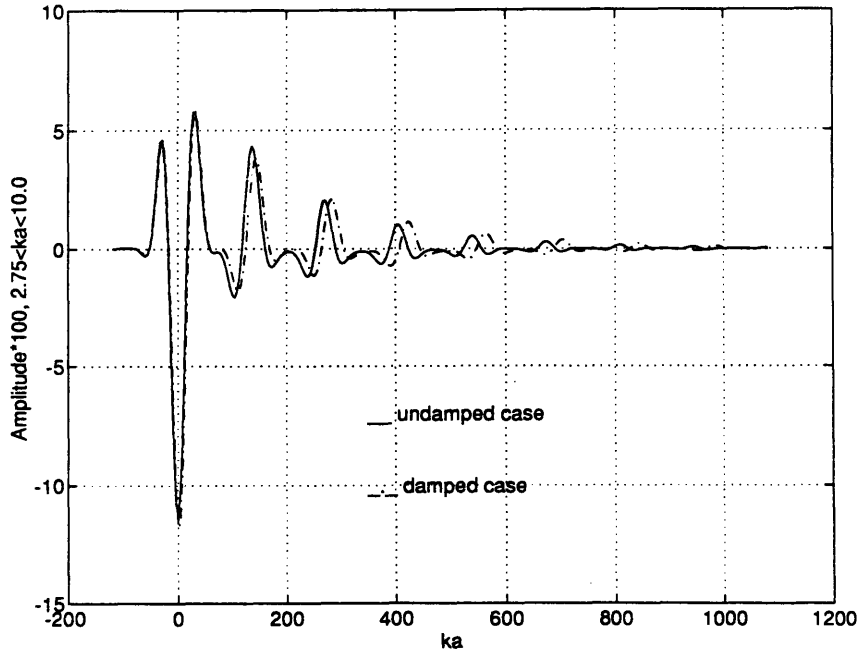

Figure 5. Back scattering form function of an undamped and damped cylindrical shell at normal incidence in the time domain. The loss factor of the visco-elastic layer of a damped shell with equal layer thickness is assumed to be one. Form function obtained through inverse transform of harmonic series solution in the frequency range from $2 < ka < 10$.

Chapter 3.

Underwater Experiments Using a Visco-Elastically Damped Shell

In the following the experimental configuration for the model testing is discussed; this includes the design parameters of the visco-elastically damped shell. Then the experimental results are analyzed by using simplified theoretical models, which include theoretical results from the thin-shell model.

3.1. Experimental Configuration

The model used in the experiments was similar to the shell-model Corrado [1] used in his experiments to explain fundamental backscattering processes. It is internally loaded with four one-inch diameter delrin rods interconnected by cylindrical steel masses. The four rods are

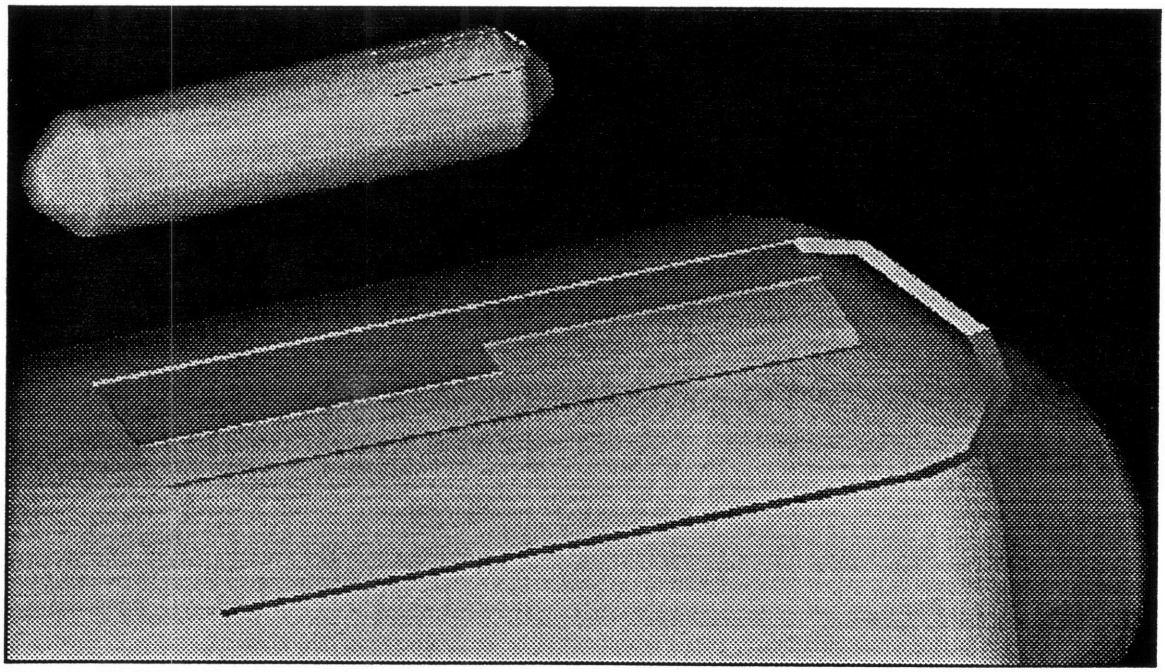

Figure 6. The visco-elastically damped shell used in the experiments.

quadrant symmetrically arranged and they are attached to the inner shell by wedge-shaped rubbers blocks. The internally loaded shell was coated on its cylindrical shell section with a visco-elastic material (EAR: C-2206), which incorporates a high loss factor and a large Young's modulus at room-temperature, the idealized shell configuration is shown in Figure 6. Then, in a second step, the outer layer was applied by shrink wrapping four small cylindrical shell sections onto the coated cylinder faces. The junctions between the outer cylinder facings, as well as the junctions between outer cylinder and endcaps, were filled with epoxy of high stiffness. The whole assembly was undertaken at the Naval Research Laboratories (NRL). The cylindrical part of the shell was ground smooth to avoid surface discontinuities. It was not possible to coat the endcaps. Therefore, there did exist a small surface discontinuity between the cylindrical section of the shell and the endcap, which, however, was smoothened through the application of epoxy. The shell, NRL model number 5100, is air-filled and has an overall length of 0.86 m and a radius of 0.0559 m. The thickness to radius ratio for the composite shell is 0.038. A summary of the design parameters for the composite shell is shown in Table 1.

On March 1994, the internally loaded model was submerged in a water tank at NRL and insonified by broadband impulse plane waves. All the receivers were located at a constant radius of 2m from the (empty) shell's geometric center in the shell plane. Measurements were conducted in one degree increments of the target angle for the monostatic backscatter measurements and similarly, in one degree increments of observation angle for specific target angles for the bistatic measurements. The data acquisition parameters, as well as the test procedures and configurations, are similar to the one's Corrado used during his experimental analysis; see Appendix B.

Table 1. Summary of Model Design Parameters

Configuration	
Face-Layer, Endcap, and Ring Material	Ni-200
Length Overall, L	0.86m
Shell Radius, a	0.0559m
Shell Thickness, h	0.0020m
Face-Layer Thickness, h^{α}	0.0005m
Core-Layer Thickness, h^{c}	0.0010m
Aspect Ratio, $L/2a$	7.7
Thickness Ratio, h/a	0.038
Approx. Shell Material Properties	
Young's Modulus of Face-Layers, E^{α}	2.2×10^{11} N/m^2
Young's Modulus of Core-Layer, E^{c}	2.0×10^{09} N/m^2
Density of Face-Layers, ρ^{α}	8900 kg/m^3
Density of Core-Layer, ρ^{c}	1200 kg/m^3
Poisson's Ratio of Face-Layers, ν^{α}	0.31
Poisson's Ratio of Core-Layer, ν^{c} (assumed)	0.40
Loss Factor of the Core-Layer (assumed)	0.7
Approx. Delrin Material Properties	
Measured Dynamic Modulus, E_{rod}	3.7×10^{9} N/m^2
Density, ρ_{rod}	1400 kg/m^3
Poisson's Ratio, ν_{rod}	0.35
Measured Compressional Speed of Rod	1625 m/s

3.2. Experimental Results and Comparison with Theoretical Results

The theoretical results indicated the possibility to attenuate the shell response of an infinitely long cylinder under plane wave excitation. However, it is up to the experiment to verify these predictions and to show whether different wave types excited on the shell can be efficiently attenuated by means of a visco-elastic, constrained layer. In the previous chapter, it was described that the specular reflecting wave field is basically not affected by any damping treatment. Therefore, in Figures 15 to 19 the specular return field was subtracted from the scatter signal in the depicted experimental data. The resulting purely elastic shell response is compared to the similarly processed response of an untreated empty and internally loaded shell.

All the experimental form functions shown in Figure 7, 9 and 10 are obtained from the measured transfer functions of the scatter and reference source signals. As shown in Appendix A1-2, Eq. (A.14), the cylindrical spreading of the wave field is accounted for by the correction $\sqrt{2r/a}$, which results in a spreading loss of 18.6 dB. An additional - geometrical - correction of $20 \log \sqrt{2.18/1.96} = 0.5$ dB for the spreading loss from the source location (2.18m from target center) to the receiver location (1.96m from target center) is used in the analysis of the experimental data.

The frequency location of the minima obtained by the theoretical thin-shell model and the transformed experimental data coincide very closely at normal incidence, see Figure 7. The results of the theoretical models are based on the assumed material properties, shown in Table 1 and they differ only in the location of the backscatter minima. The full-elastic model overpredicts the frequencies of the shell resonances as seen in the comparison of the theoretical and experimental results. However, a parametric analysis has shown, that the location of these pressure minima are highly dependent on the correct specification of material properties used as an input

into the theoretical models. But the real material properties are not known to such a high degree, that this shift in frequency between models would matter.

The levels for the experimental scattering pressure recorded at beam incidence are elevated, in comparison to the theoretical results.

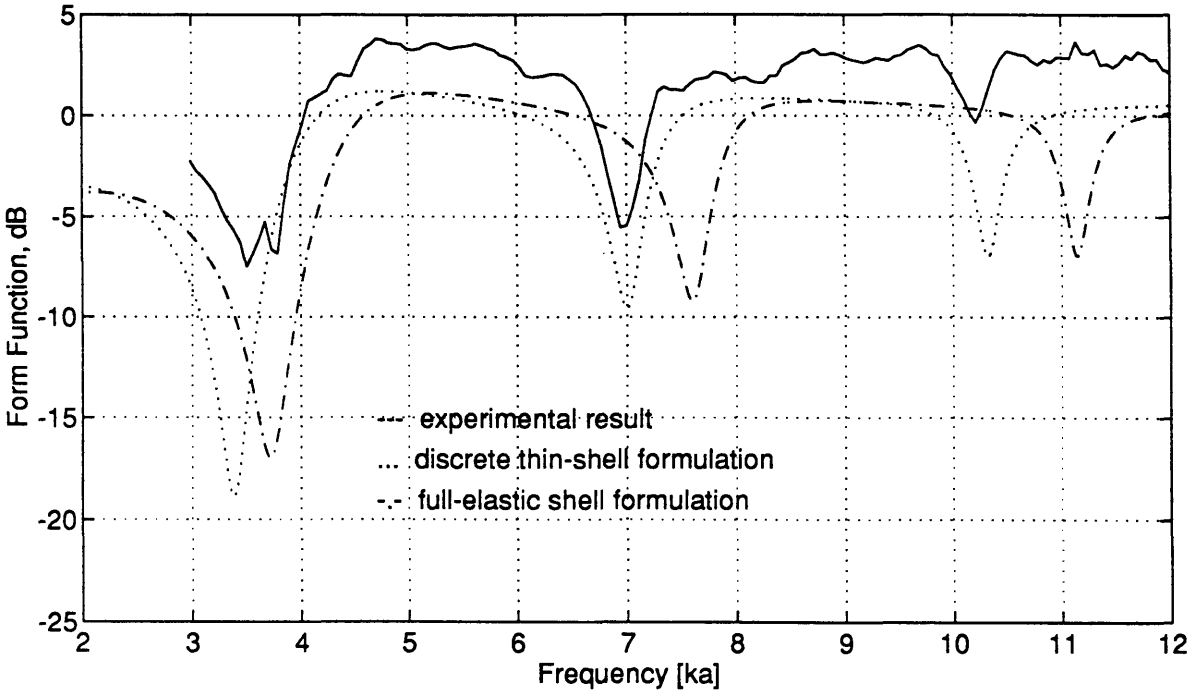

Figure 7. Monostatic spectral response of the visco-elastically damped shell at normal incidence. The theoretically and experimentally obtained form functions are shown in the frequency domain.

Corrado [1] found the same phenomenon in a comparison of experimental data between the empty and the internally loaded shell. He found that the measured backscatter of the empty shell is slightly increased (approx. 2-3 dB) for frequencies from ka = 3.5 to ka 5.5 as compared to the theoretical results for the infinite shell. In addition, he showed that above a threshold frequency of ka = 5.5 the internal loadings do increase the backscatter. Neither the thin-shell nor the full-elastic theory employ the coupling of internals to the shell, and therefore, this has to result in different backscatter levels if compared to experimental data.

The bandlimited impulse response of the damped shell at normal incidence (beam aspect) is shown in Figure 8; it was obtained by a deconvolution process of the source signal from the receiver signal at a radius of r = 2 m.

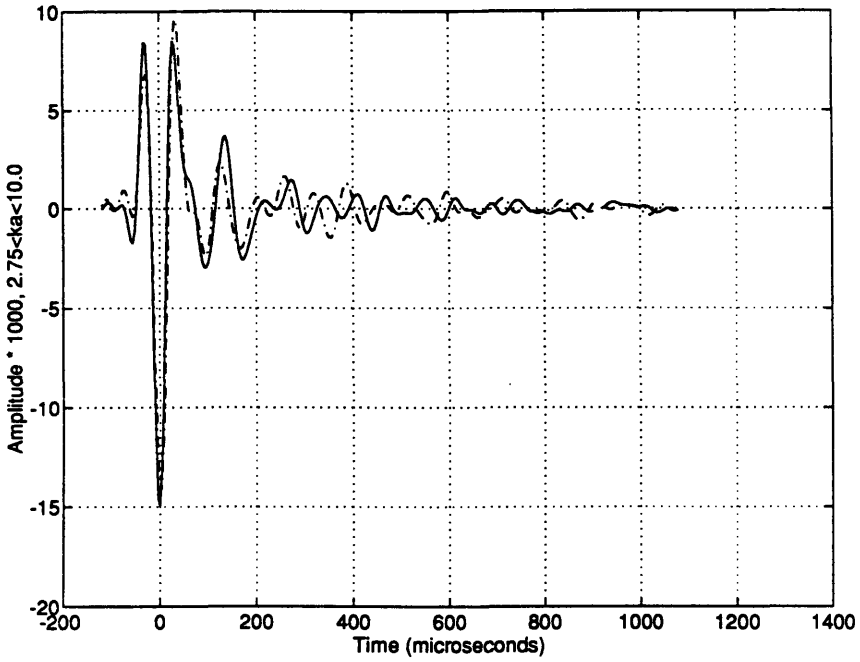

Figure 8. Gaussian bandlimited monostatic impulse response of the internally loaded and the visco-elastically damped shells at normal incidence. The form function is obtained by inverse transform in the frequency range of 2.0 < ka < 10.0.

It is seen in Figure 8, that the pressure levels for the damped shell are reduced as compared to the pressure levels for the undamped shell. The scattering pressure of the damped shell was recorded at a radius of 2m. According to Steinberg [9] the criterion for the far field assumption is met at a radius of $r \succ L^2/\lambda$. Therefore, the measurement was not done in the Fraunhofer or far field for the source frequencies employed in this experiment, which range from approximately 9 kHz to 50 kHz. A frequency dependent correction must be applied to the target strength estimation of the damped shell in the far field. Corrado [1] developed a simple discrete line array model to estimate this correction factor. If this correction is of importance, it can be

easily incorporated in the scattering results. However, the frequency dependent correction factor is omitted in Figures 8 and 9, which depict the attenuation effect of the damping layer at normal incidence. Figures 12, 15 and 16 show the target strength of the internally loaded and damped shells for aspect angles ranging from zero to 90 degrees. The target strength, $T(\theta)$, was computed from the measured transfer functions of the measured monostatic receiver and source pressures,

$$T(\theta) = 10 \log \frac{\int_{\omega} P^2_{Receiver}(\omega,\theta)\, d\omega}{\int_{\omega} P^2_{Source}(\omega)\, d\omega} . \qquad (19)$$

As discussed above a spreading correction of 0.5 dB and a cylindrical spreading loss of 6 dB is included in the shown target strength calculations. The frequency dependent correction factor is not incorporated in the depicted data. However, its spectral representation is shown in Figure 25 in Appendix A1-2; it was computed by using Corrado's line array model.

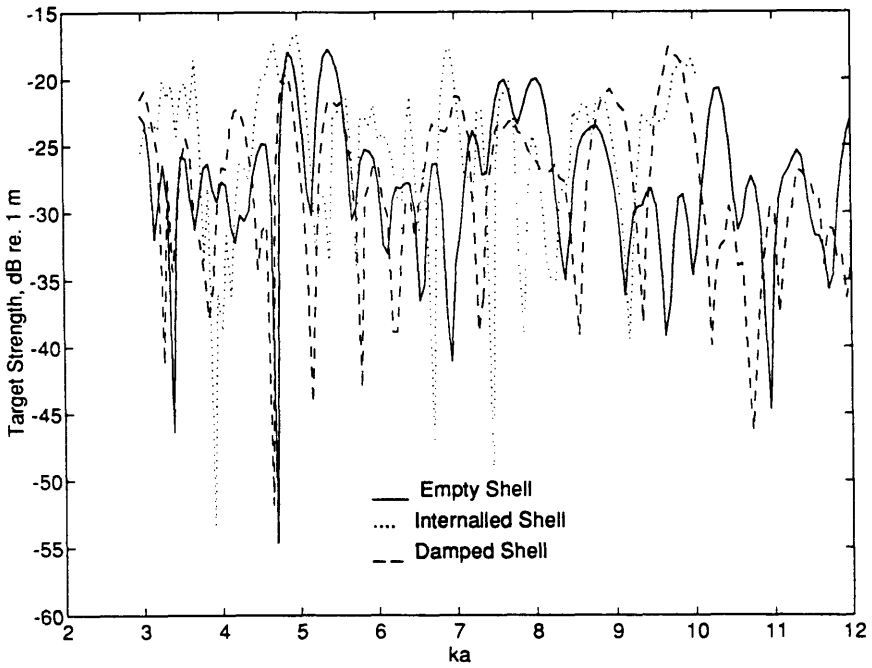

Figure 9. Comparison of the measured target strengths of the empty, internalled, and damped shell at an incidence angle of 75 degrees; frequency dependent correction factor not included.

Figure 9 shows that, at beam incidence, the first minimum value of the experimentally determined target strength of the damped shell is deeper cut than the minimum associated with the untreated shell. An analysis of the theoretical results of a constrained-layer shell with different shell thickness to radius ratios reveals that the deeper cut associated with the damped shell is due to the higher shell thickness to radius ratio if compared to the same ratio of the untreated internalled shell; see Figures 2 and 3. The theoretical results also show a shift of the locations of the minima to slightly higher frequency values. However, the experimental values for the target strength do not confirm this tendency, as a matter of fact, the minima, which are located above ka = 5, occur at lower frequencies as the comparable internalled shell,.see Figure 9. The overall levels of damped and internalled shell in a frequency range of ka = 4 to ka = 10 are similar in value.

It can be concluded from the scattering results in the frequency domain that only small damping will occur for a visco-elastically damped shell at normal incidence. If the shell is excited at angles where shear waves are dominant i.e., at incidence angles ranging from approximately 60 degrees to 80 degrees, then the damping treatment will show a significant increase in its attenuation effect.

The analysis of the measured monostatic back-scattering pressure for an incidence angle of 75 degrees, Figure 10, demonstrates the effective damping of shear waves in this region. The direct comparison of results between damped and untreated shells shows a decrease in backscattering levels over a wide frequency band. Especially scatter of low and mid frequencies appear to be damped quite efficiently. The high frequency scattering levels are very similar in the undamped and damped case. If compared with the empty shell surprising analogies in the signal envelope occur at and around specific frequencies, such as ka = 3.5 and from approximately ka

= 4.7 to ka = 6. These analogies will be visible also in the time-history plots of the experimental data, where the response of the damped shell looks similar to the response to an untreated empty shell.

The envelope of the backscatter at 75 degrees aspect angle is depicted in a time-history plot in Figure 11. Again the response of the untreated and the damped shell are plotted on the same axis.

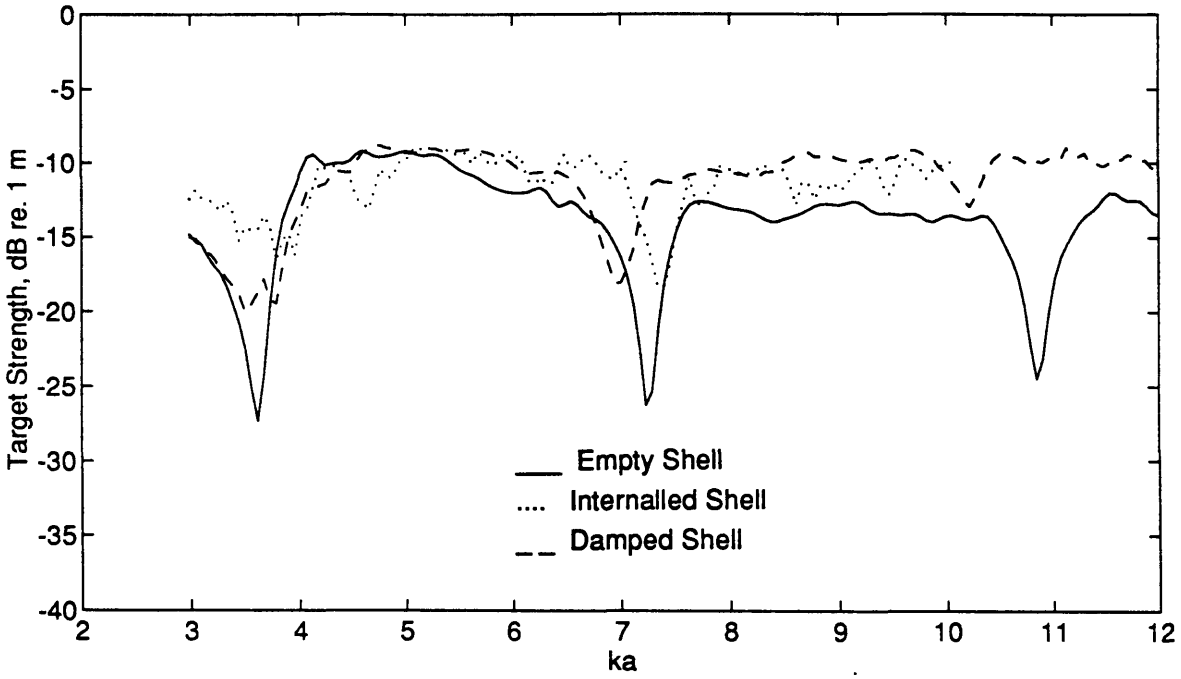

Figure 10. Comparison of the measured target strengths of the empty, internalled, and damped shell at normal incidence; frequency dependent correction factor not included.

It is interesting to see the change in target strength if the specular return signal is included and if it is removed. The target strength for the damped and untreated shells over aspect angles ranging from 0 degrees to 90 degrees and which include the specular return signal is shown in Figure 12. As can be seen in Figure 12, the overall target strength is reduced over all aspect angles.

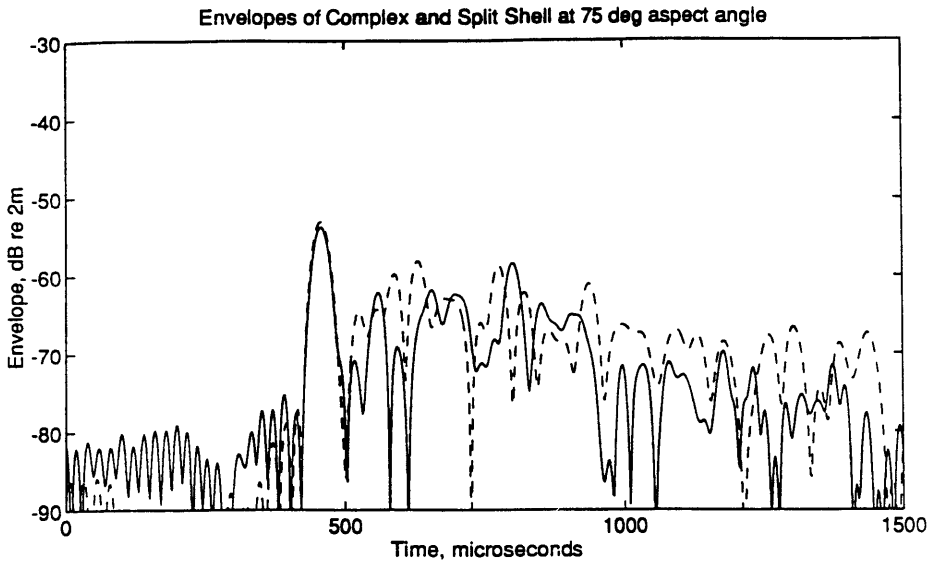

Figure 11. Magnitude of the envelope of the gaussian bandlimited impulse response of the untreated (dashed line) and damped shell at an incidence angle of 75 degrees; frequency range of gaussian filter from ka = 2.75 to ka = 10.0; radial distance r = 2 m from target center.

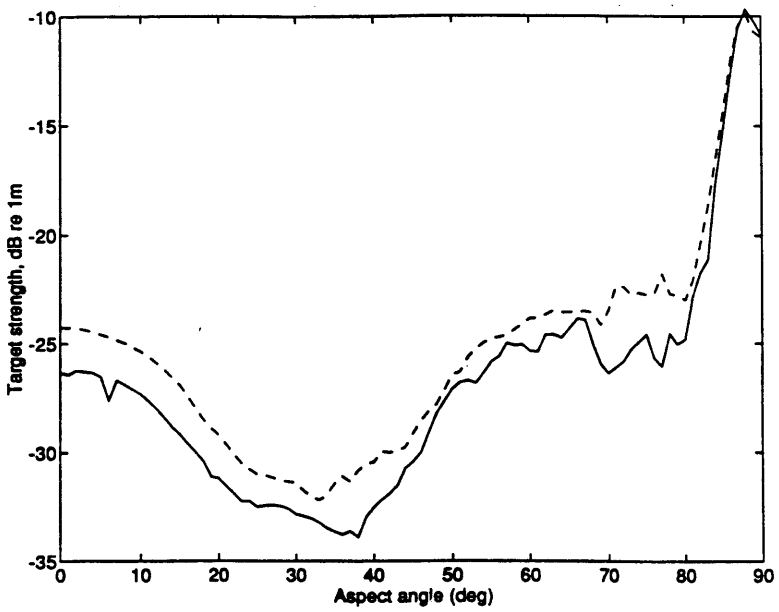

Figure 12.. Integrated target strength of the untreated (dashed line) and the damped shell over a frequency range of ka = 2.75 to ka = 10.0 for a region of aspect angles ranging from 0 to 90 degrees; specular return signal was not removed from shell responses.

The magnitude of the envelopes of the response of untreated and damped shells for specific aspect angles are shown in Figure 13 and the magnitude of the target strengths in the frequency domain are shown in Figure 14. All scattering representations in Figures 12 to 14 include the initial, specular scattering signal and all scattering signals show a reduced elastic shell response for the visco-elastically damped shell.

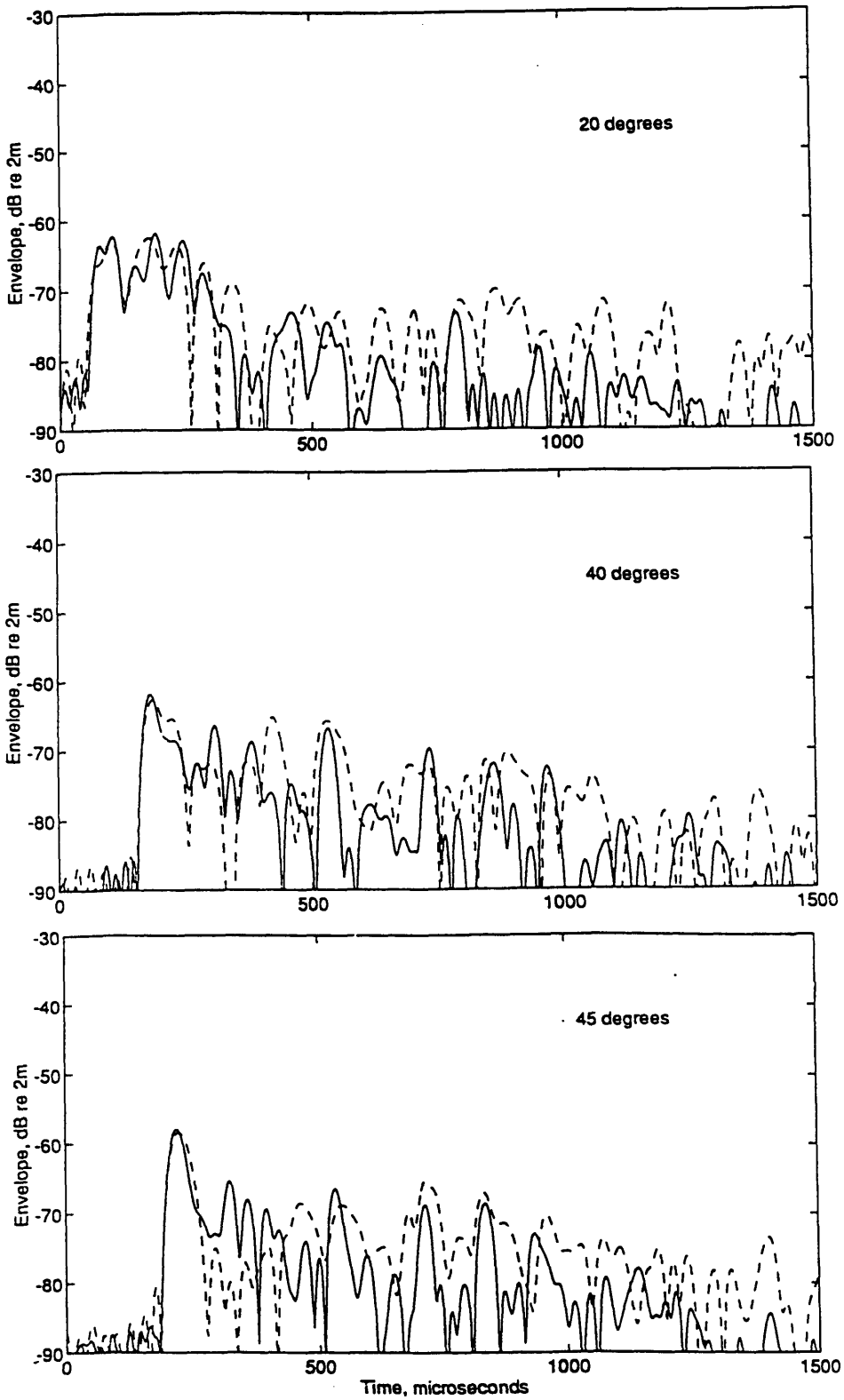

Figure 13. Magnitude of the envelopes of the gaussian bandlimited impulse response of the untreated (dashed line) and damped shell for specific angles of incidence; frequency range of gaussian filter from ka = 2.75 to ka = 10.0; radial distance from target center r =2 m.

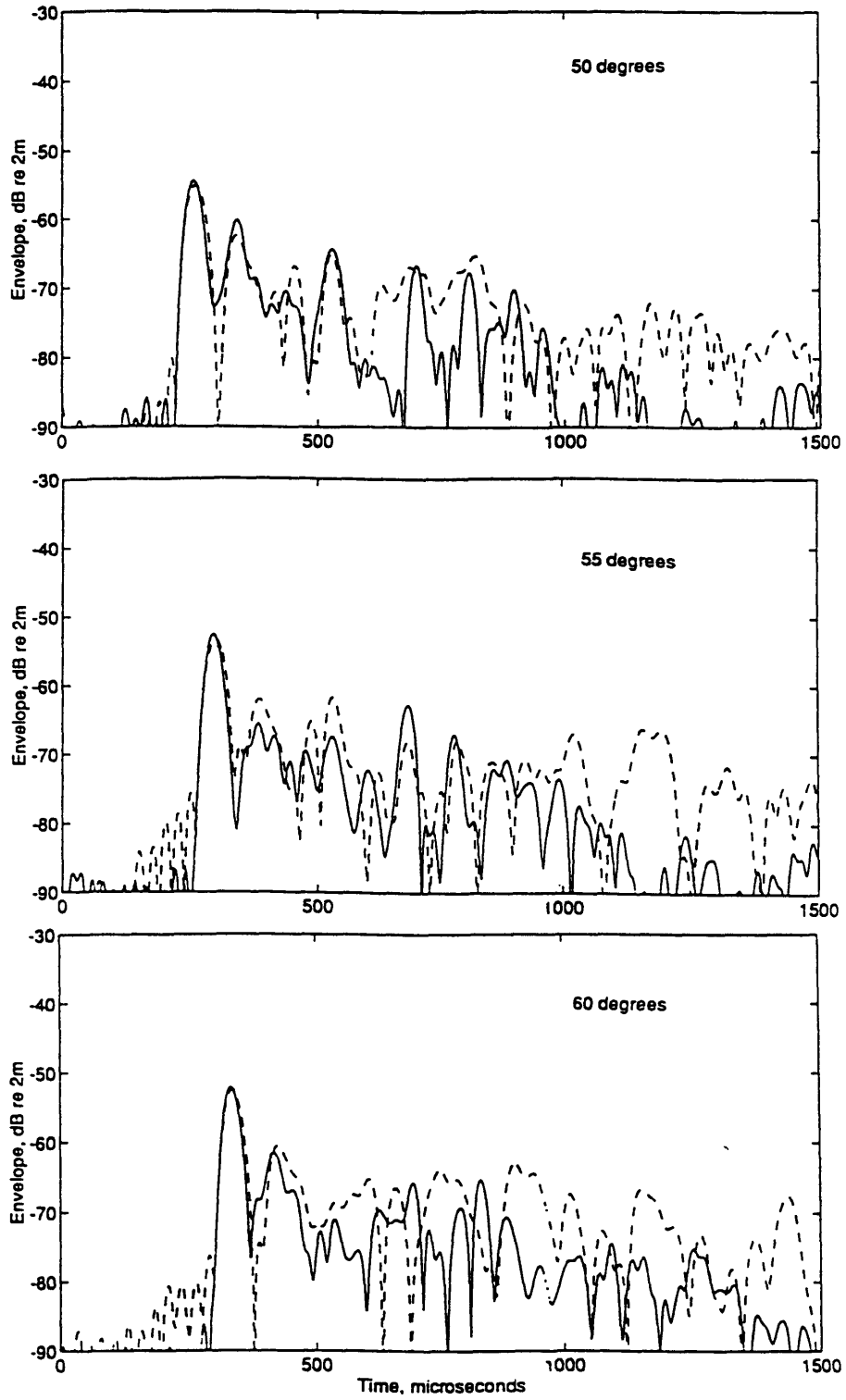

Figure 13 (continued). Magnitude of the envelopes of the gaussian bandlimited impulse response of the untreated (dashed line) and damped shell for specific angles of incidence; frequency range of gaussian filter from ka = 2.75 to ka = 10.0; radial distance from target center r =2 m.

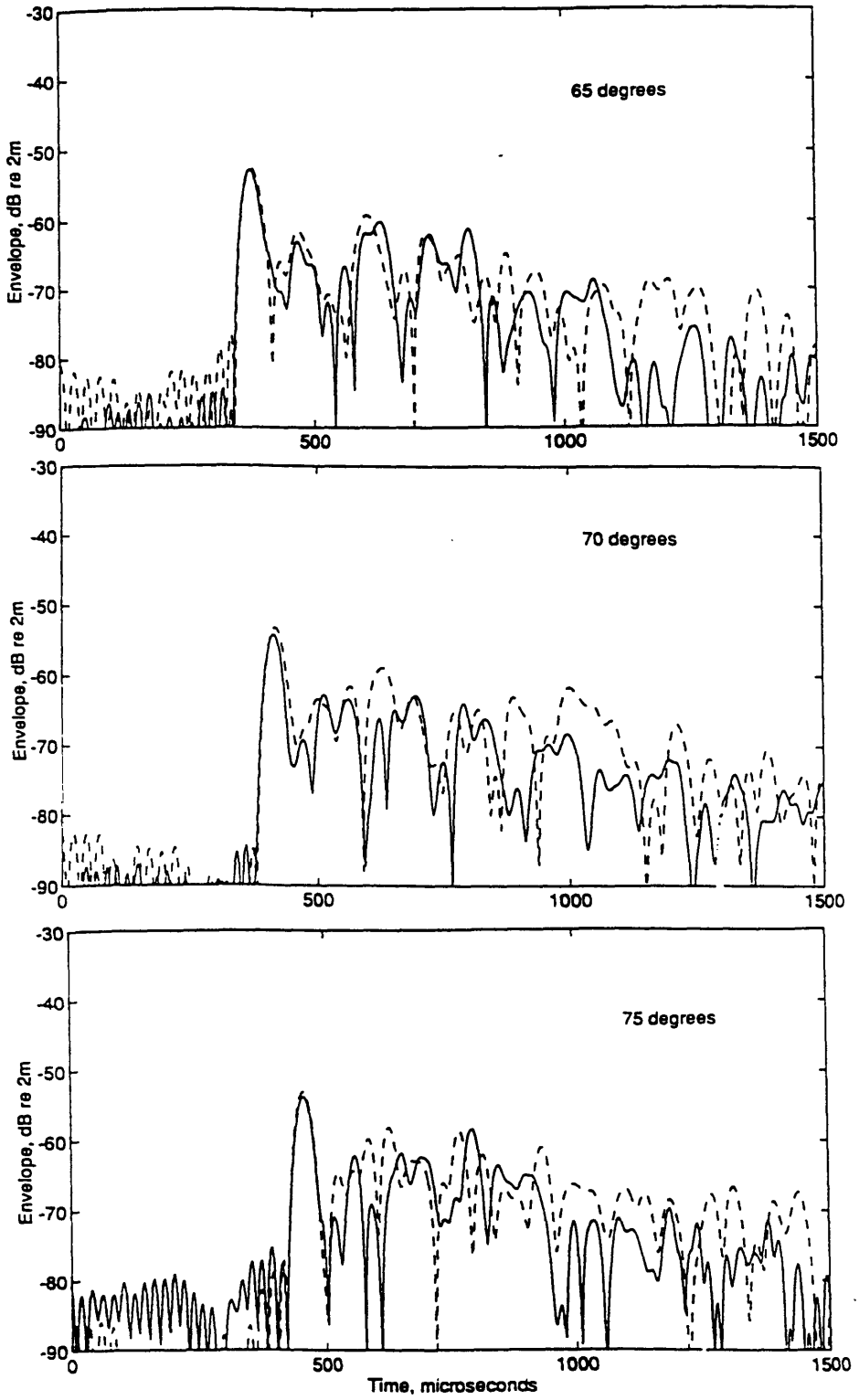

Figure 13 (continued). Magnitude of the envelopes of the gaussian bandlimited impulse response of the untreated (dashed line) and damped shell for specific angles of incidence; frequency range of gaussian filter from ka = 2.75 to ka = 10.0; radial distance from target center r =2 m.

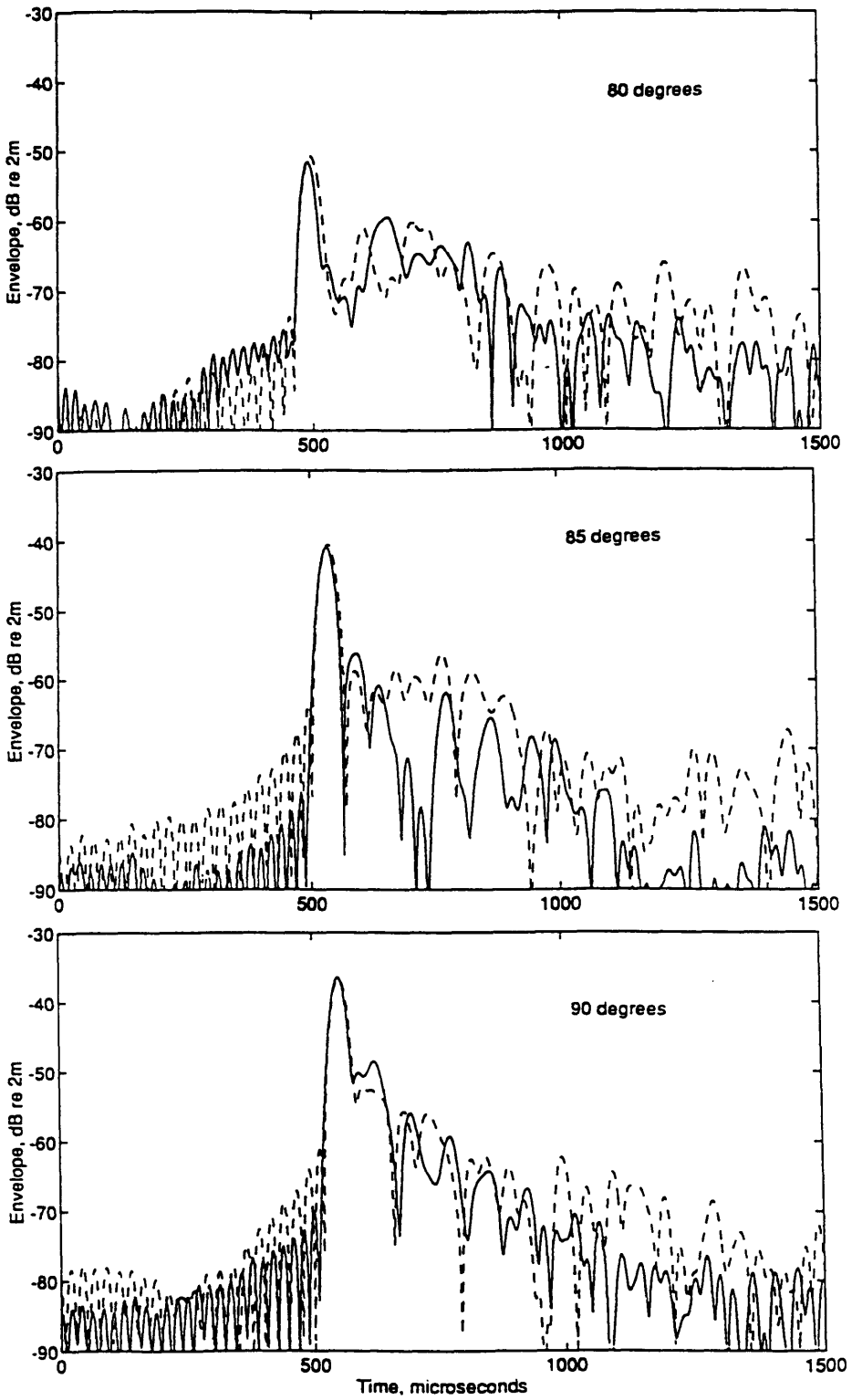

Figure 13 (continued). Magnitude of the envelopes of the gaussian bandlimited impulse response of the untreated (dashed line) and damped shell for specific angles of incidence; frequency range of gaussian filter from ka = 2.75 to ka = 10.0; radial distance from target center r =2 m.

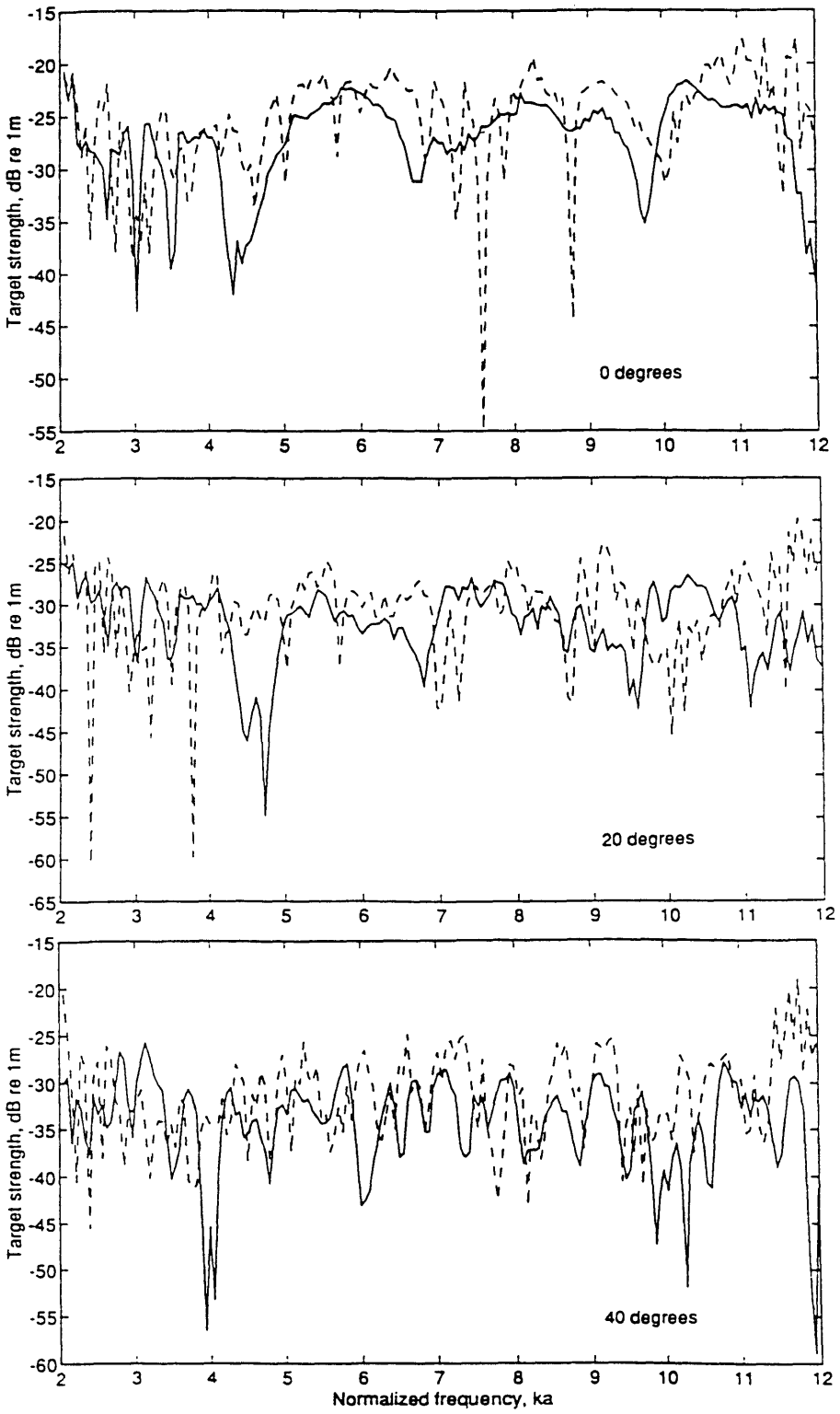

Figure 14. Target strength for the untreated (dashed line) and the damped shell for specific angles of incidence; frequency range of gaussian filter from ka = 2.75 to ka = 10.0; radial distance from target center r = 1 m.

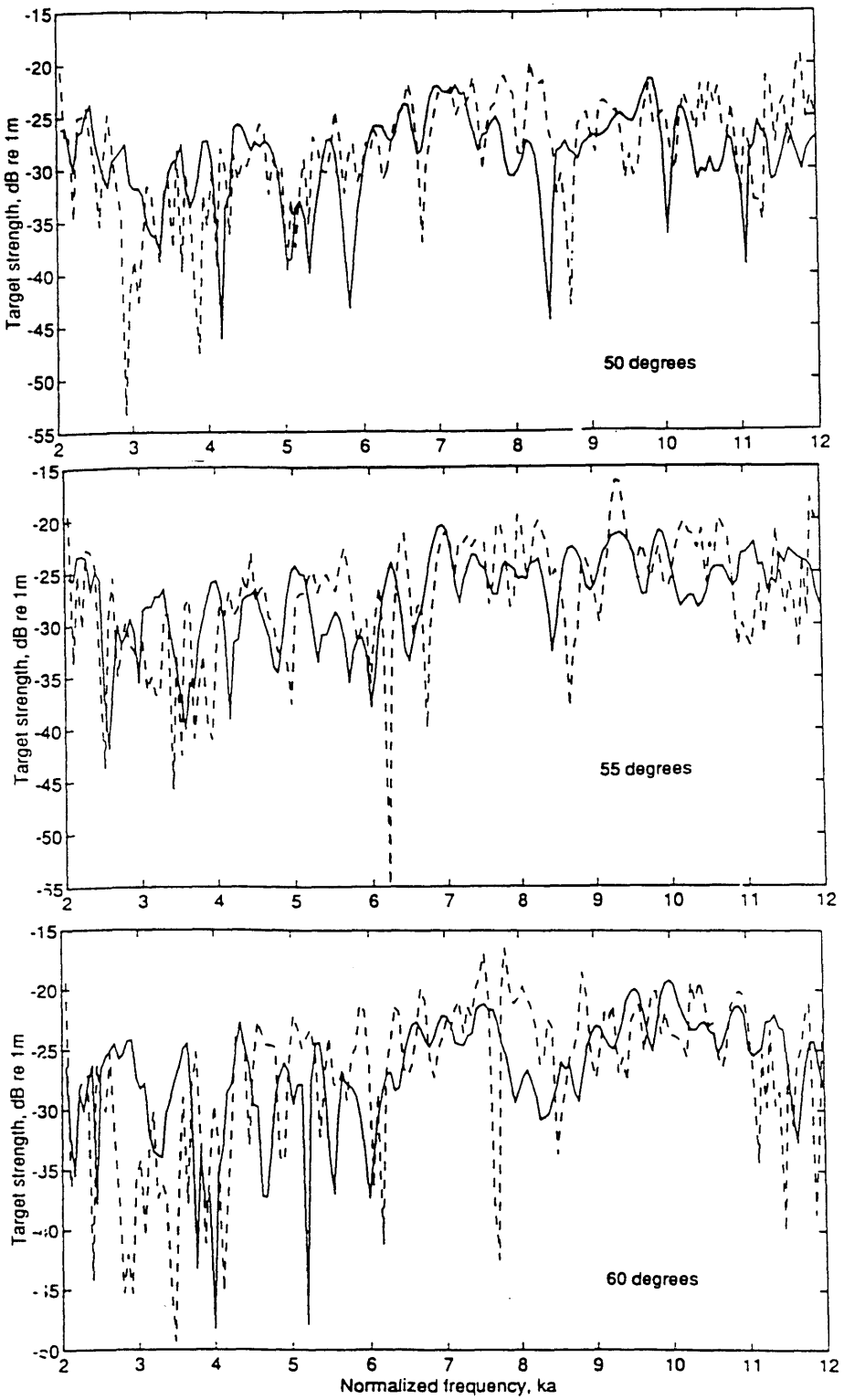

Figure 14 (continued). Target strength for the untreated (dashed line) and the damped shell for specific angles of incidence; frequency range of gaussian filter from ka = 2.75 to ka = 10.0; radial distance from target center r = 1 m.

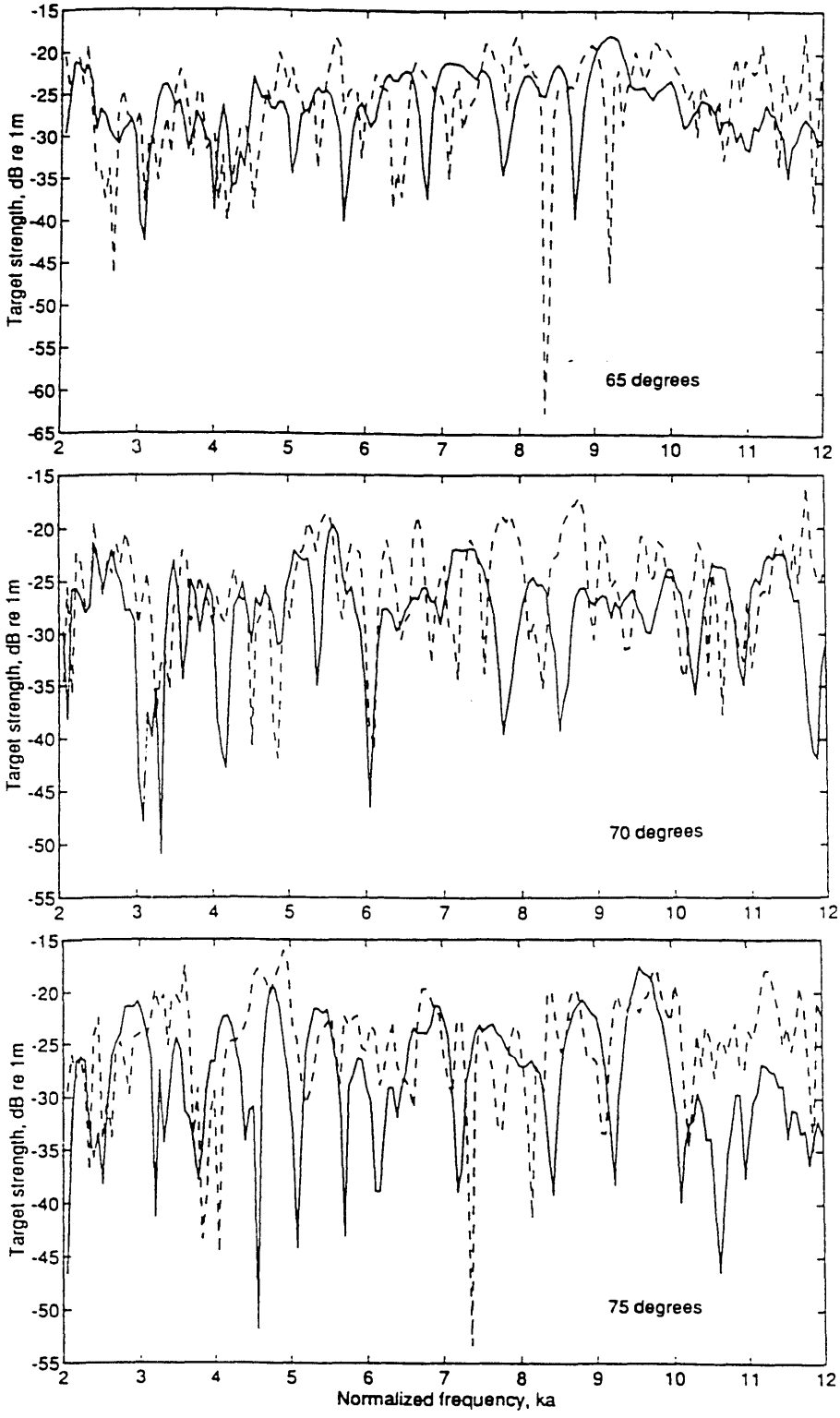

Figure 14 (continued). Target strength for the untreated (dashed line) and the damped shell for specific angles of incidence; frequency range of gaussian filter from ka = 2.75 to ka = 10.0; radial distance from target center r = 1 m.

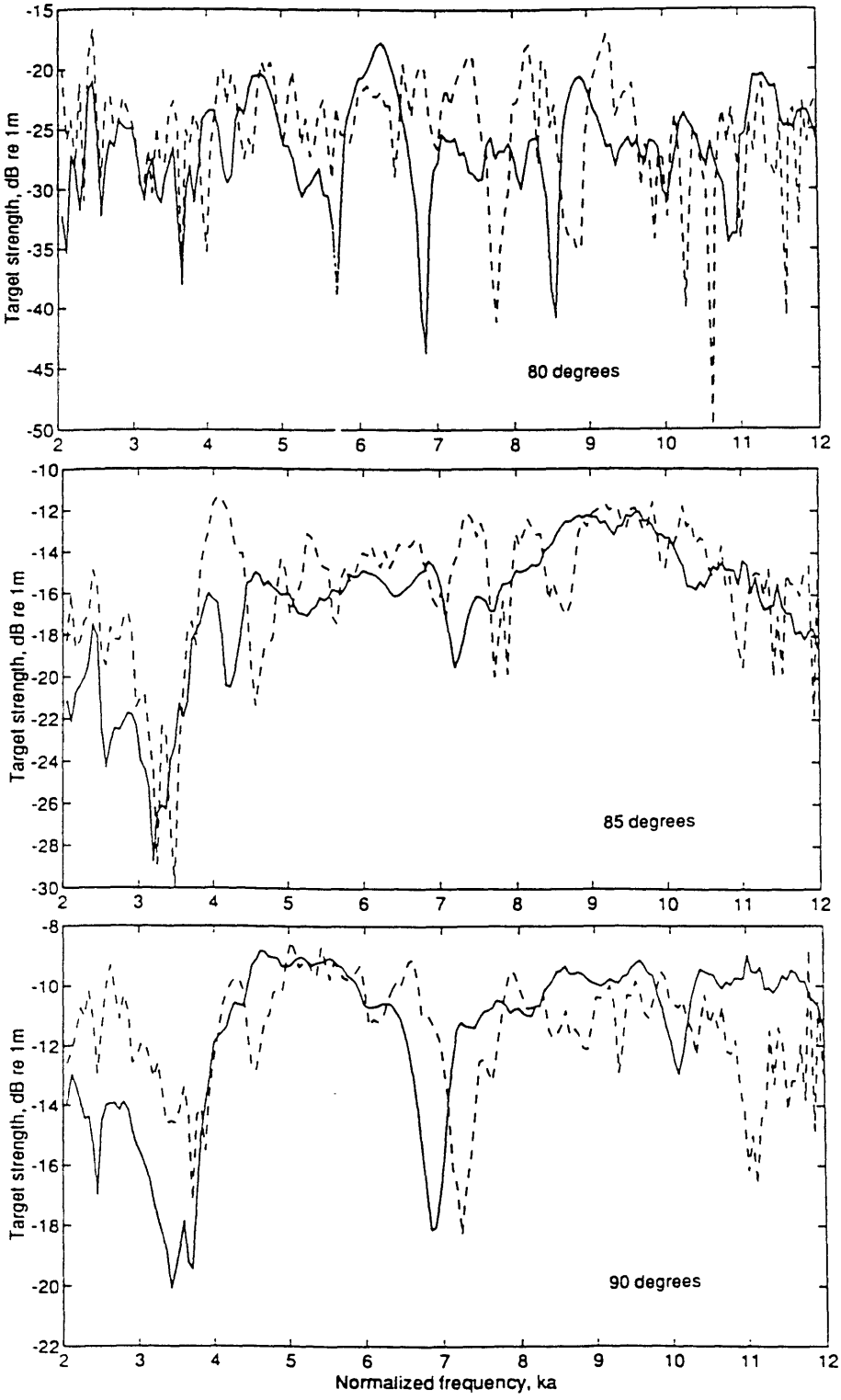

Figure 14 (continued). Target strength for the untreated (dashed line) and the damped shell for specific angles of incidence; frequency range of gaussian filter from ka = 2.75 to ka = 10.0; radial distance from target center r = 1 m.

The integrated target strengths with the specular return removed for the untreated and damped shell over a range of aspect angles are shown in Figure 15 and show a significant reduction in the backscatter for the damped shell. The specular return signal is removed in the depicted data for the target strength in Figure 15, because only the elastic shell response occurring later in time can be effectively damped and the initial, unaffected specular return signal should not be integrated in the target strength calculation.

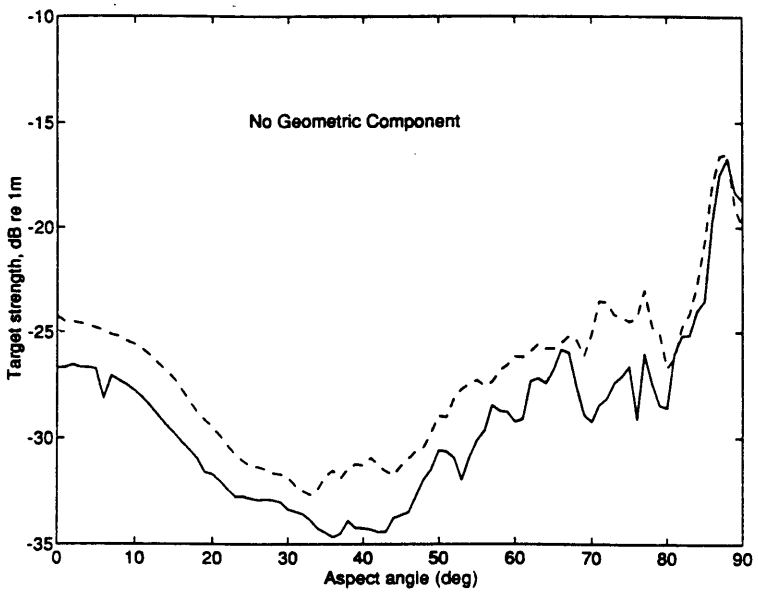

Figure 15. Integrated target strength of the untreated and the damped shell over a frequency range of $2.75 < ka < 10.0$ for a region of aspect angles ranging from 0 degrees to 90 degrees; specular return signal removed of shell responses.

Conti [10] compared the initial target strength for different shells including the untreated and the damped shell. He found that the target strength values for the initial return differ slightly at 0 degree aspect angle. However, it is known that all shells have identical endcaps and if insonified at bow aspect (0 degrees) should generate the same target strength values. Therefore he concluded, that the difference in target strength is due to a measurement calibration error. As a result, the target strength values for both shells were corrected by subtracting -3dB from the

target strength for the damped shell and -1dB for the untreated shell to compensate for this calibration error, see Figure 16.

Figures 17 to 18 depict the results in the time domain for different aspect angles. The displayed data show a strong attenuation for specific angles and time regimes. The comparison between the untreated shell, see Figure 17, and the treated shell, see Figure 18, reveals that at bow incidence, both compressional and flexural waves are more strongly attenuated in the damped shell. As a consequence, the scattering off the first and all following internal rings is significantly reduced. The back scattering signal which is associated with the endcap only are not significantly affected as seen in the time regime smaller than 70 microseconds.

The region between 20 degrees to 60 degrees reveals the importance of the direct back scattering off both the rings and the discontinuities on the shell, such as junctions between the cylinder and the endcaps. The arrival times at the sensor provide patterns, which extend diagonally from 90 degrees aspect angle and time zero to about 15 degrees and times ranging from 200 to 1000 microseconds. The loci of these patterns coincide with the calculated delays corresponding to direct acoustic scatter off the rings and discontinuities, as shown by Corrado [1]. The elastic response of the damped shell is attenuated in a region starting from 60 degrees to about 90 degrees for time beyond 150 microseconds.

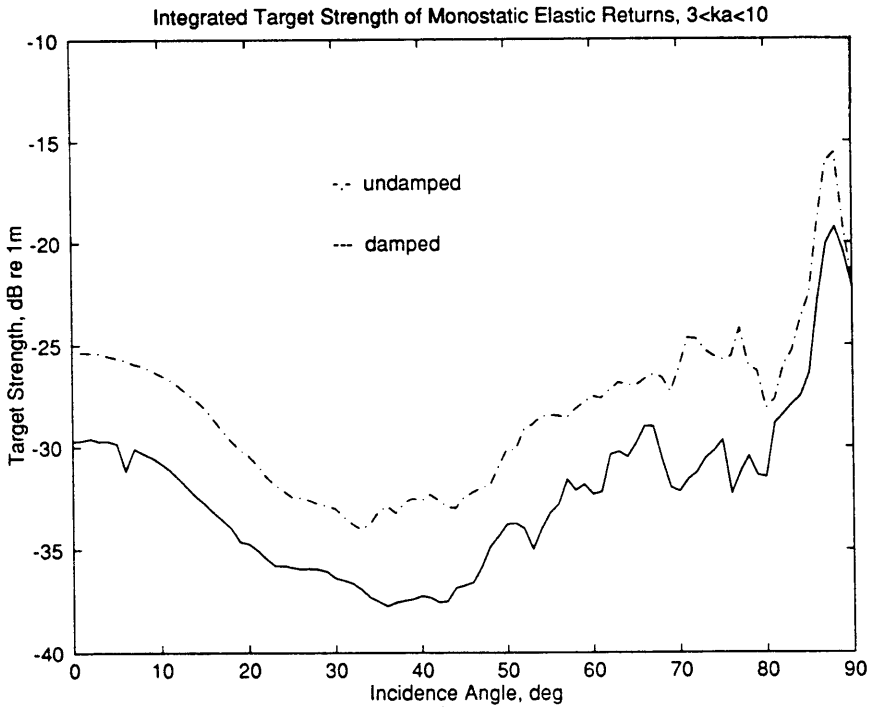

Figure 16 Corrected integrated target strength of the untreated and the damped shell over a frequency range of $2.75 < ka < 10.0$ for a region of aspect angles ranging between 0 degrees to 90 degrees; specular return signal removed of the shell responses; target strength values corrected using initial specular return, frequency independent correction -1 dB for the untreated shell and -3 dB for the damped shell.

A difficult to interpret interference pattern exists in the range of 60 to 85 degrees, where shear wave contributions and scatter off the rings overlap. In the region between 85 and 90 degrees aspect, the compressional wave contribution are noticeably attenuated.

An anomaly should be noted in the scattering data in Figure 18; for an aspect angle of six degrees the magnitude of the pressure is not correct due to incorrect hydrophone readings. This anomaly appears in the integrated data of the target strength calculations, Figures 12, 15 and 16.

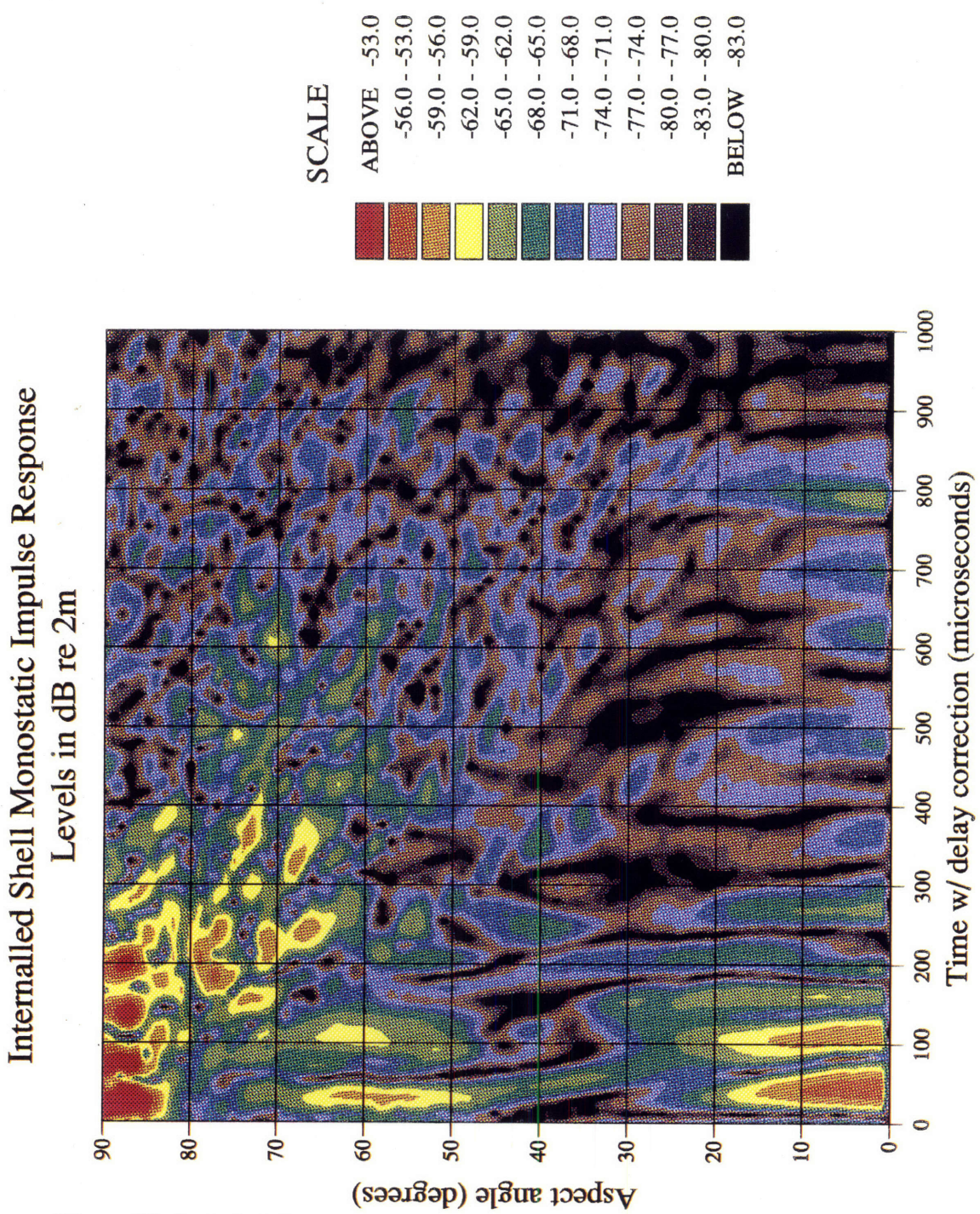

Figure 17. Analytical signal envelope of the gaussian bandlimited monostatic impulse response for the untreated shell at r = 2 m for a frequency range of ka = 2.75 to ka = 10.0 and aspect angles from θ = 0 degrees (bow aspect) to θ = 90 degrees (beam aspect or normal incidence). The specular return signal and the time delay for the shown angles are removed in the data set.

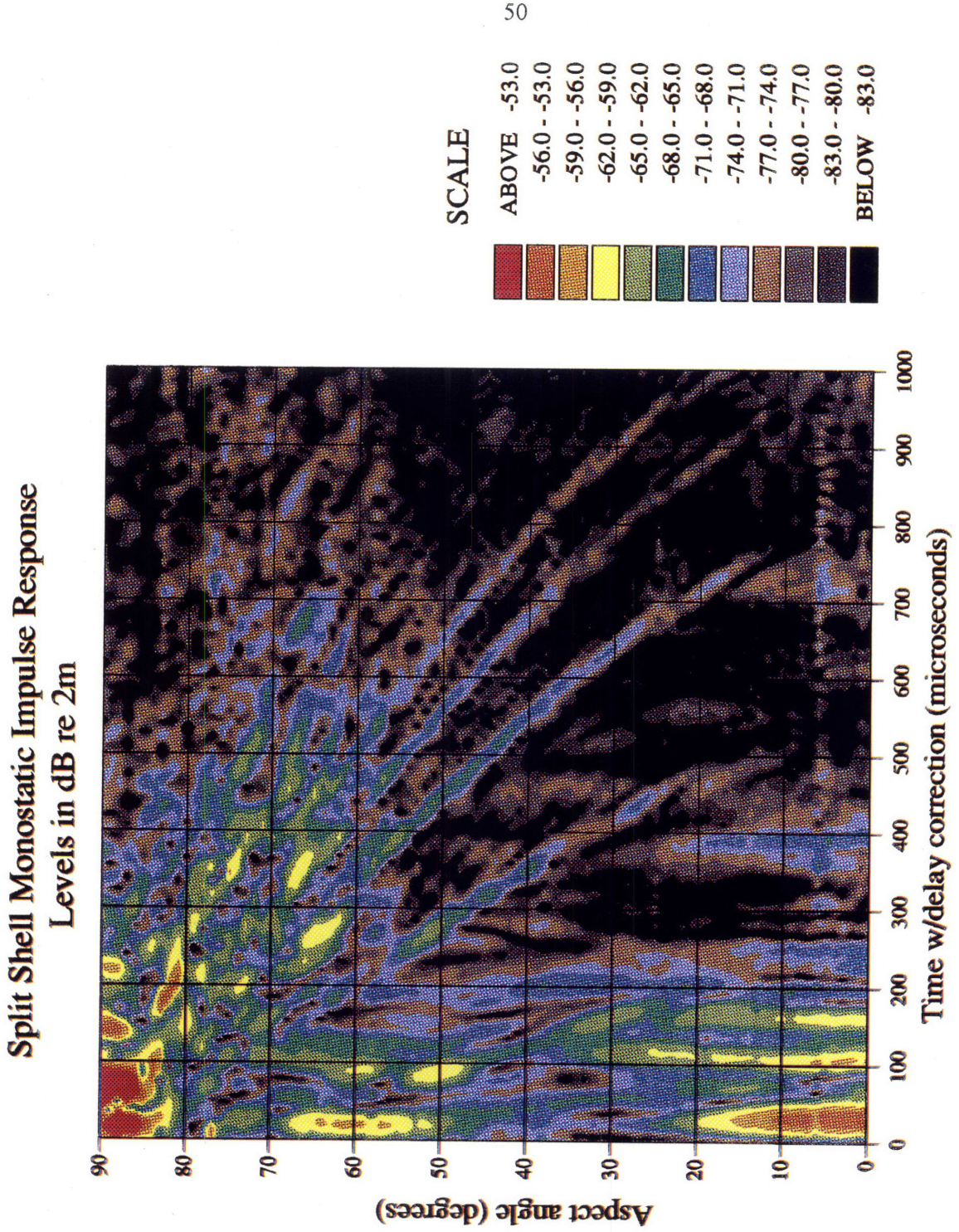

Figure 18. Analytical signal envelope of the gaussian bandlimited monostatic impulse response for the damped shell at r = 2 m for a frequency range of ka = 2.75 to ka = 10.0 and aspect angles from θ = 0 degrees (bow aspect) to θ = 90 degrees (beam aspect or normal incidence). The specular return signal and the time delay for the shown angles are removed in the data set.

The same overall reduction in the backscattering can be seen in the comparison of the responses in the frequency domain for the two shells studied (the specular return is removed in Figures 19 and 20). At all aspect angles, there is a reduction in target strength over the entire frequency band. For aspect angles of 60 to 85 degrees, in which the overall backscatter is clearly reduced. The shear wave loci corresponding to order $n = 2$ are still clearly visible; these are extending diagonally from about 90 degrees aspect angle and a frequency of ka = 4 to about 60 degrees aspect angle and ka = 7. The shear wave loci corresponding to orders $n = 1$, 3, and 4 run parallel to the $n = 2$ shear wave, but are not as prominent. These wave types are created by the outer shell.

As seen in the time history plots, Figures 17 and 18, the aspect angles from about 15 to 60 degrees are strongly attenuated and mainly influenced by the backscattering from the rings. The pattern seen in Figure 20 represents the direct acoustic scatter off the shell rings and local discontinuities. This effect is more clearly visible in the time domain, see Figure 18. The influence of the rings on the acoustic behavior is also prominent at a target angle of 75 degrees and visible in the time domain representation of the bistatic field generated by the visco-elastically damped shell, see Figure 22. At this selected angle both shear and compressional waves are excited on the shell and radiate out into the fluid. Strong scattering levels are observed at the shear wave coincidence loci, ranging from 60 to 90 degrees. A direct comparison of the scattering levels between undamped and damped shell, see Figures 21 and 22, reveals lower scattering levels for the damped shell as expected, which illustrates the successful damping of these waves in the angular region of excitation.

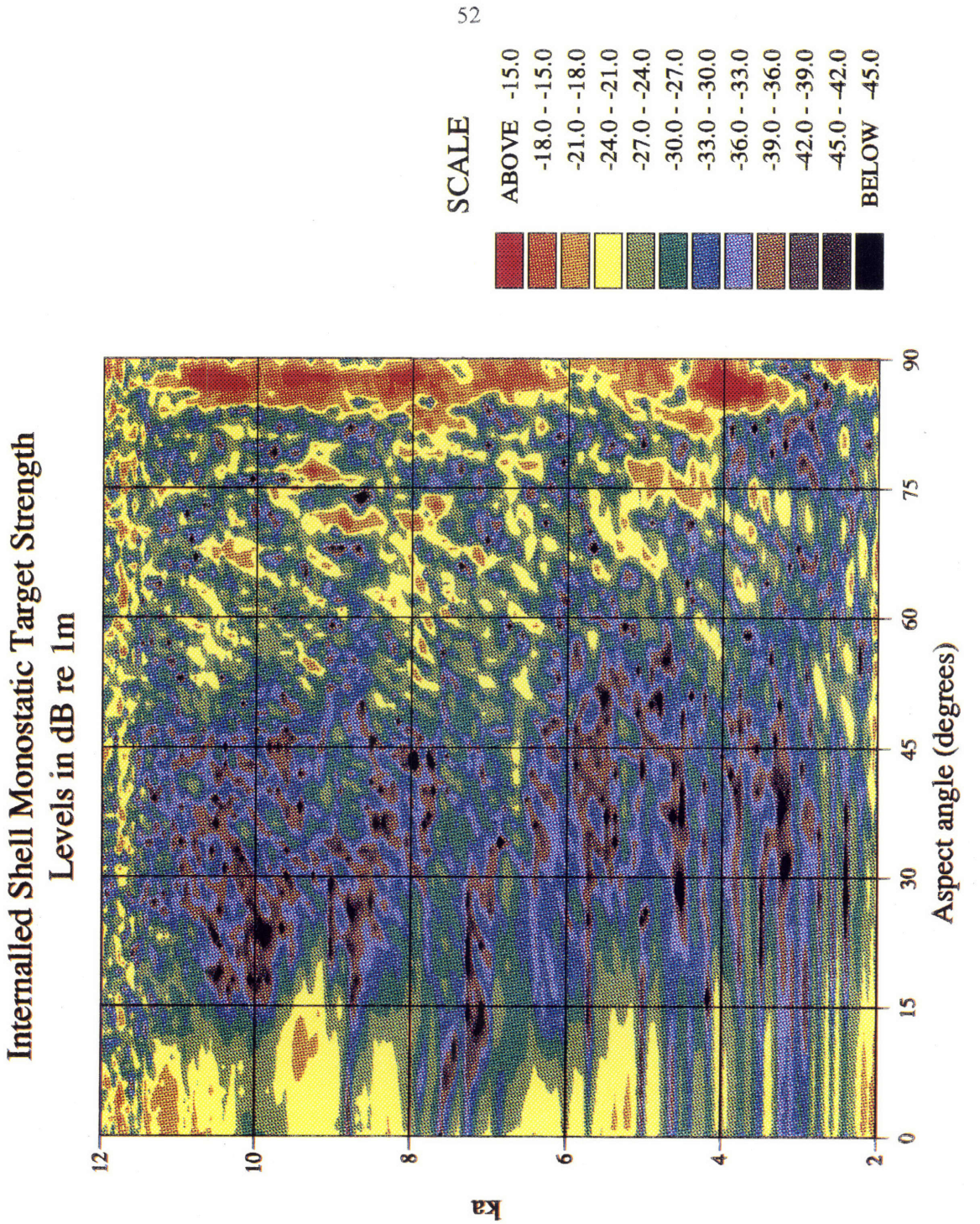

Figure 19. Monostatic target strength of the untreated shell over the region of aspect angles, ranging from $\theta = 0$ degrees to $\theta = 90$ degrees; target strength values are normalized by the pressure level of the incidence field at the target center location.

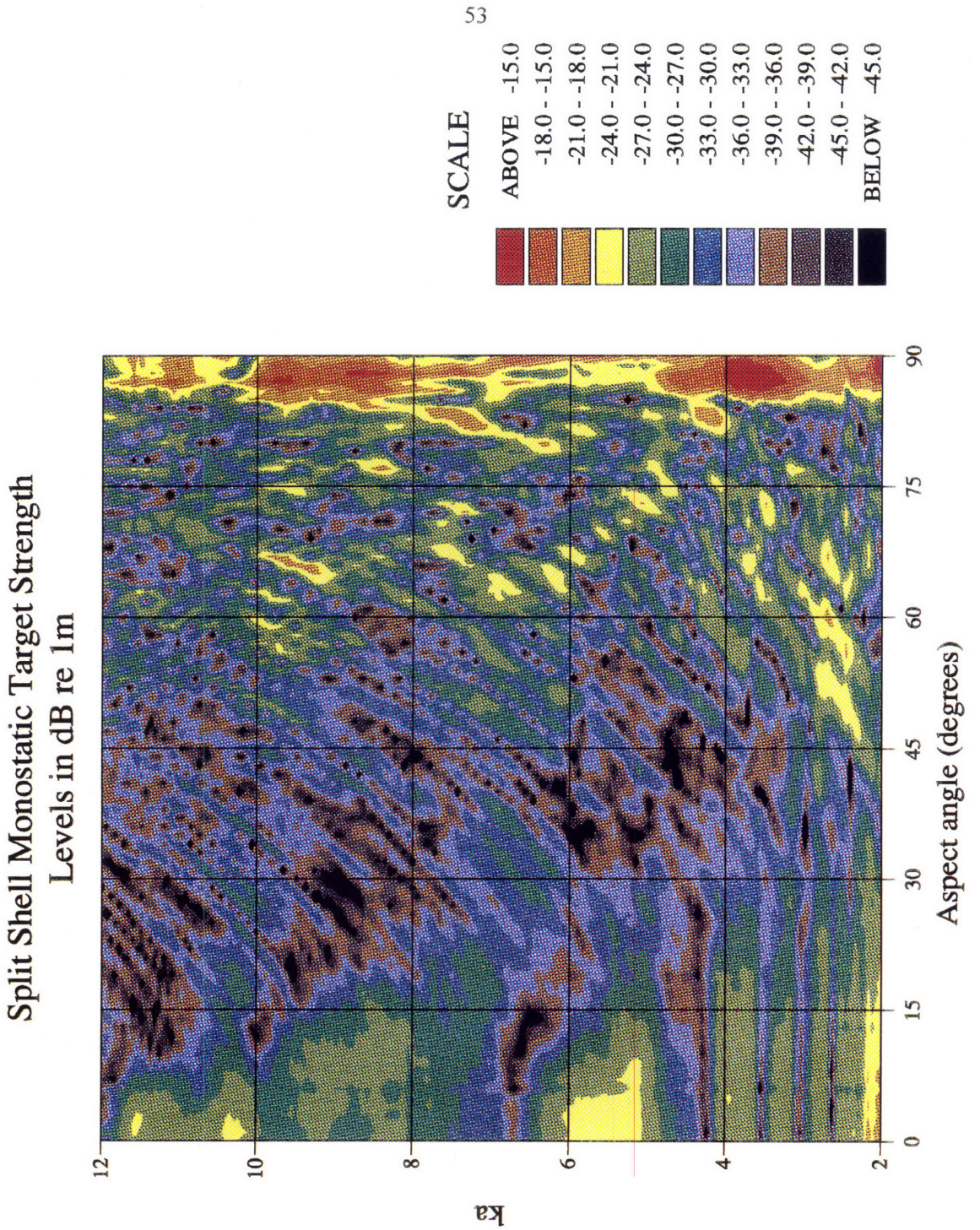

Figure 20. Monostatic target strength of the damped shell over the region of aspect angles, ranging from $\theta = 0$ degrees to $\theta = 90$ degrees; target strength values are normalized by the pressure level of the incidence field at the target center location.

The specular return in the region between 35 and 55 degrees depicted in Figure 18 shows higher scattering levels, this is mostly likely due to the geometric discontinuity on the outside of the shell, located between the cylindrical section and the endcap of the experimental shell. In the region between 0 degrees and approximately 60 degrees the acoustic scatter off the internal rings is very prominent in the damped shell response. In order to study the time evolution of the bistatic scatter off the rings a simple array model was developed which allows for prediction of the direct scatter off the rings and the first reflection from one ring to the next ring. Figure 23 depicts the physics of the direct scatter off the rings and the evolution of the subsequently induced elastic waves on the shell surface. Figure 24 shows the computed time evolution of the scattering pressure.

In both the damped and undamped shell the excited shear and compressional waves scatter off the rings and radiate into the fluid. The loci in time for the scatter off the rings are identical for both shells. However, the scattering pressure levels of the damped shell created by the internal rings, are slightly higher for the damped case. This is most likely due to the higher shell thickness and as a consequence a higher impedance at the ring locations, which induces higher scattering levels in the far field. Further, the ring scatter is overlapped with additional wave contributions in the undamped case, which do not appear in the response of the damped shell.

There is a strong scatter off the first ring in a region from 45 degrees to 70 degrees. A comparison between predicted and measured arrival times at an aspect angle between 38 degrees and 48 degrees shows that in addition to the direct scatter off the first ring there is also a strong scatter from the backwards reflected wave off the first ring towards the endcap. The backward scatter off the second ring appears in the bistatic field of the damped and undamped shell and stretches from an aspect angle of 45 degrees and an arrival time of 350 microseconds to an aspect angle of 0 degree and an arrival time of 250 microseconds. The direct scatter off the

second ring again is slightly higher in the damped case than in the undamped case. The direct scatter off the third and fourth rings is slightly higher than in the undamped case, as discussed before.

Backward scatter arising from these rings appear in an angular domain from 50 degrees to 90 degrees, but are difficult to detect near beam incidence. High scattering levels appear near beam incidence and times beyond the arrival time of the scatter of the far away endcap (time > 550 microsecond) for the damped shell, as depicted in Figure 22. The time loci of these levels coincides with the time loci of the scattering levels obtained by an empty shell [1]. It can be assumed that near beam incidence, these loci correspond to arrival times of shear waves generated by flexural waves traveling on the conical section of the endcap towards the spherical section, reflecting backward off the spherical part of the endcap, and finally scattering off the geometric discontinuity between the conical and cylindrical section of the shell at total times equal to the average arrival time of the specular return (at beam incidence: t = 350 microseconds) plus the traveling time of the shear wave (at beam incidence: Δt = 200 microseconds). The physical process is shown in Figure 25 for the bistatic measurement configuration.

It cannot be determined for sure, whether this scatter is caused by the slope discontinuity between the conical and the cylindrical section of the shell or whether it is caused by the impedance discontinuity between the endcap and the visco-elastically damped cylindrical section of the shell. This endcap-scatter can be observed for aspect angles ranging from 60 degrees to about 90 degrees, which corresponds to the cutoff aspect angle for shear waves. Scattering levels located later in time, beyond arrival times of 800 microseconds over all aspect angles show a strong attenuation as compared to the undamped shell.

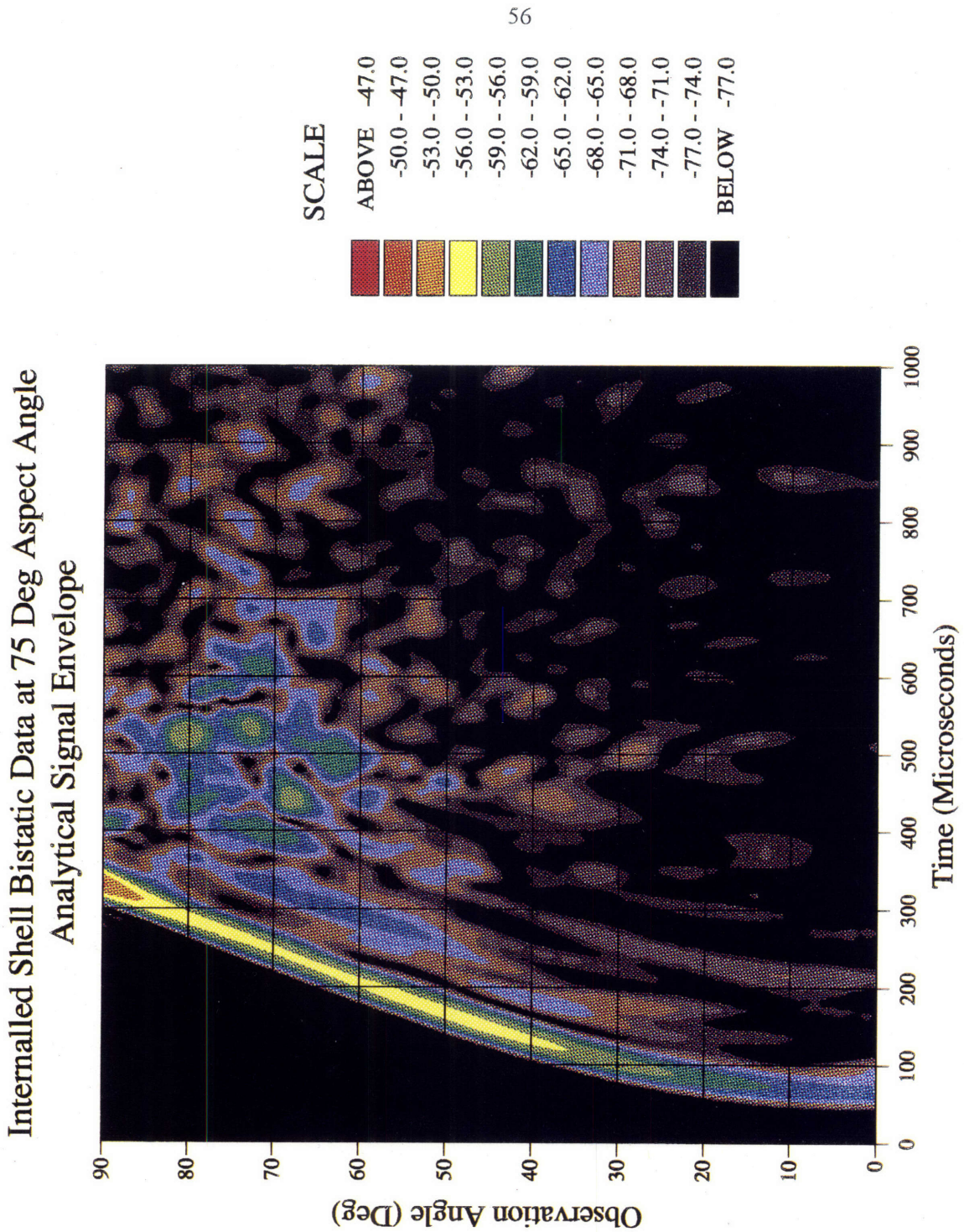

Figure 21. Analytic signal envelope of the gaussian bandlimited bistatic impulse response for the untreated shell at r = 2 m for a frequency range of ka = 2.75 to ka = 10.0 and aspect angles from θ = 0 degrees to θ = 90 degrees (normal incidence). The aspect angle of 75 corresponds to the backward specular direction.

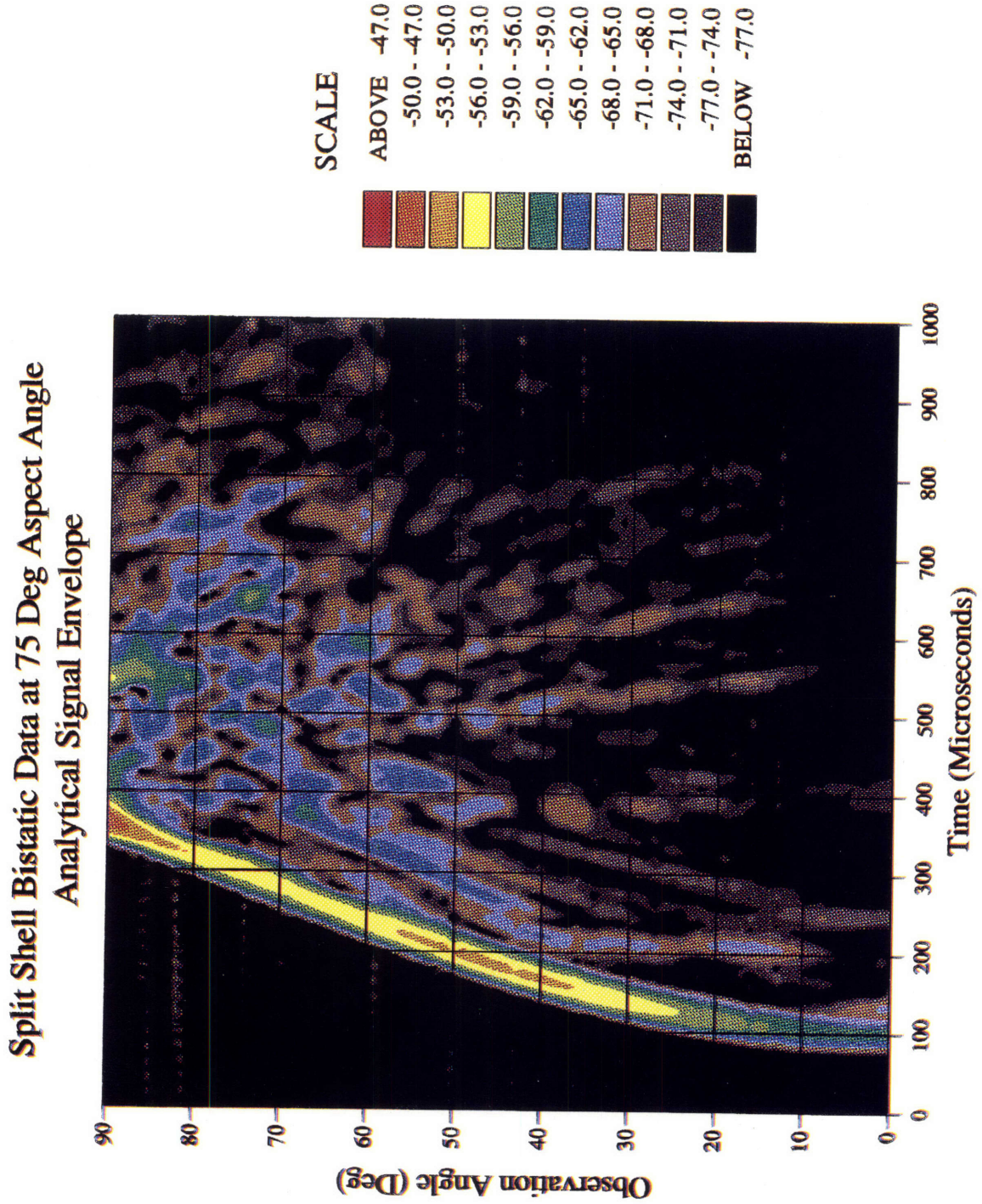

Figure 22. Analytic signal envelope of the gaussian bandlimited bistatic impulse response for the damped shell at r = 2 m for a frequency range of ka = 2.75 to ka = 10.0 and aspect angles from θ = 0 degrees to θ = 90 degrees (normal incidence). The aspect angle of 75 corresponds to the backward specular direction.

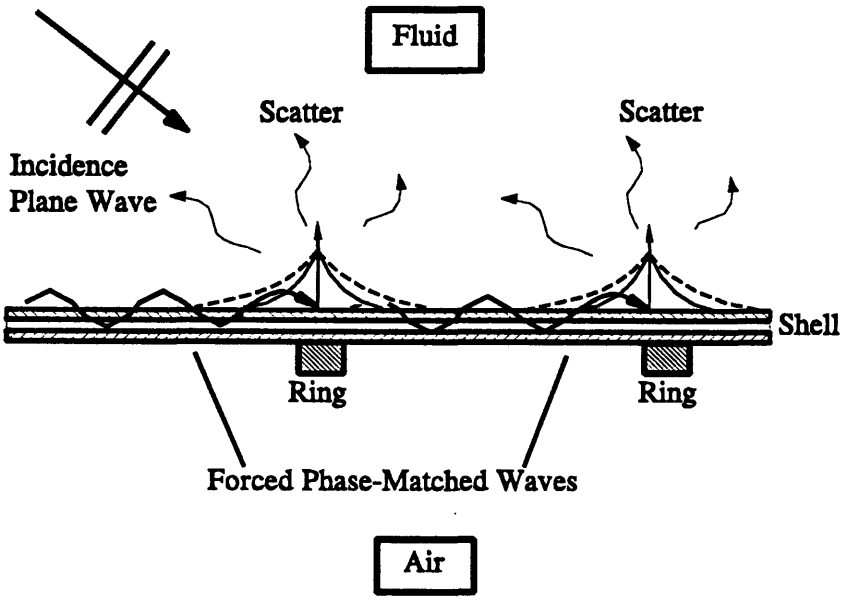

Figure 23. Direct scatter off the rings; amplitudes of elastically excited waves are more attenuated due to the constrained-layer shell design; wave amplitudes of untreated shell, - -, and damped shell, ---.

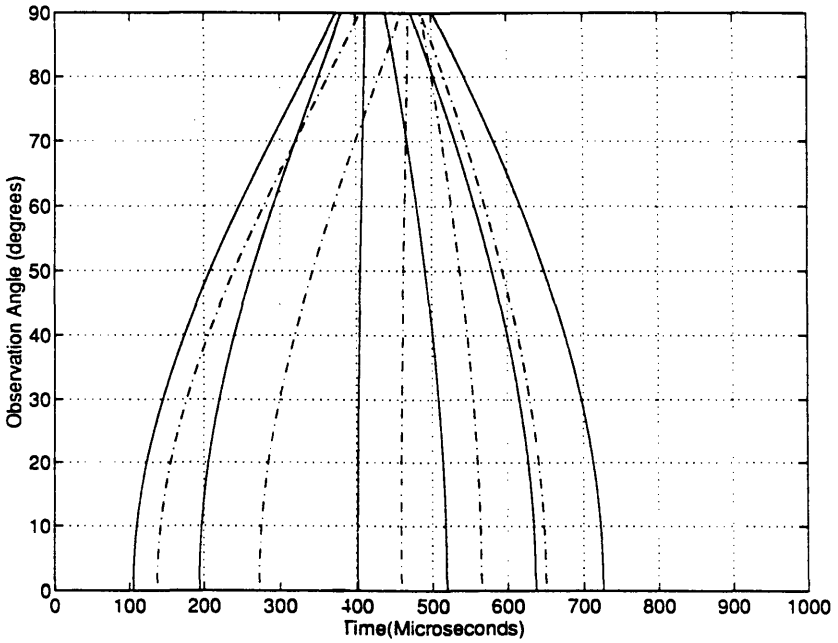

Figure 24. Predicted arrival times for the bistatic field at a target angle of 75 degrees and r = 2 m for the damped shell. Depicted is the direct scatter (solid line) off the rings and endcaps and the first backward reflection (dashed line) of a ring/endcap to the next ring/endcap. The arrival times are calculated for a axial propagation velocity which equals the trace velocity of the incident field.

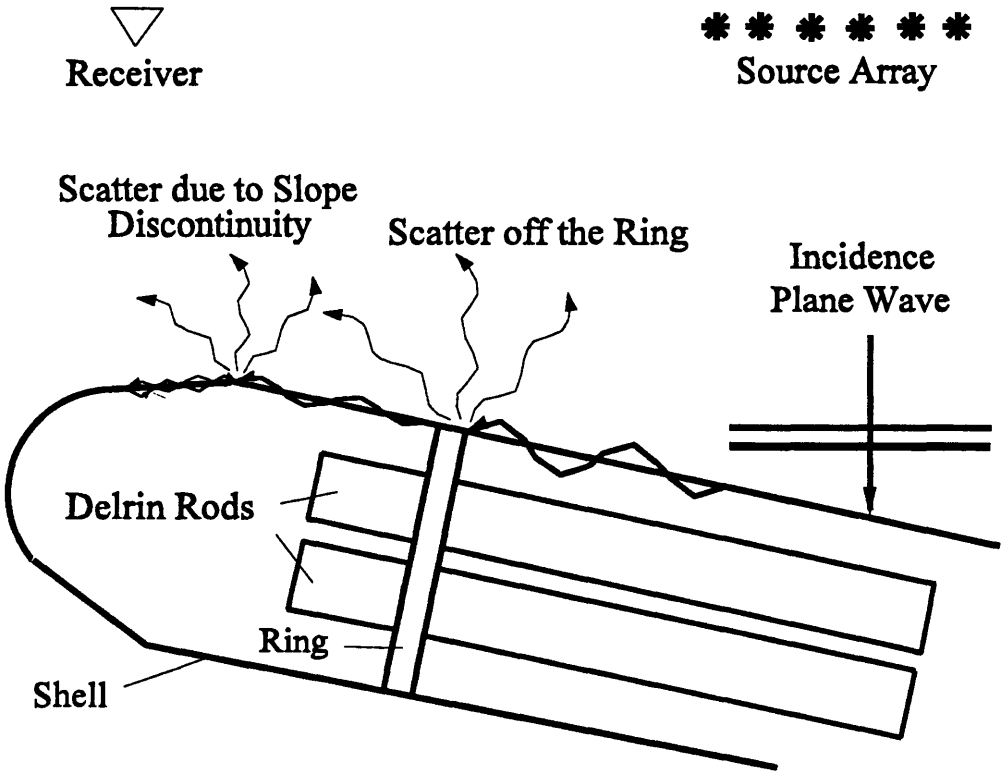

Figure 25. Acoustic scatter off impedance discontinuity on shell surface due to waves traveling in the opposite direction to the moving direction of the plane wave (backward reflected waves). As the wave is traveling in backward direction, wave energy is converted from a supersonic wave (traveling on cylindrical part of the shell) to a subsonic wave (flexural wave, conical section); the subsonic wave vertexes and scatters at the slope discontinuity between conical and cylindrical section of the shell.

Chapter 4

Conclusions

Experimentally obtained scattering levels of a visco-elastically damped and internally loaded shell were compared against the scattering levels of an untreated and internally loaded shell of similar dimensions. In addition, theoretical results were used to explain experimental observations. The primary goal of the damping treatment is the attenuation of shear waves of internally loaded cylindrical shells. The results demonstrate clearly that this goal was fully achieved. As shown in Figure 18, the visco-elastic layer effectively attenuates the shear waves in the critical region of excitation ranging for angles of incidence between 60 degrees to 90 degrees. The secondary goal of attenuating compressional waves of internally loaded shells was also achieved, as demonstrated in Figure 18 for angles around bow incidence. This conclusion can be drawn from the analysis of the monostatic, as well as the bistatic scattering fields.

Another important fact, which was observed first by Corrado, has significance again: Scatter caused by waves traveling on the shell and reflecting from attachments of internal structures to the shell is detectable in the far field. The damped shell brings out this feature in the backscatter even stronger - not through an increase in pressure level of the backscatter (the scattering levels are similar in strength), but through a very prominent scattering pattern. This can be seen clearly in the comparison between the damped and the undamped shell responses. In the undamped case, multiple reflections of supersonic waves from shell discontinuities are characterizing the shell response in an angular region of 60 degrees to 90 degrees. The damped shell attenuates the membrane waves effectively, which lose their energy quickly as they travel on the shell surface, and this attenuation effect brings out the underlying direct backscatter levels

of waves propagating in the axial direction and directly scattering off the internal rings. This effect is clearly seen by comparing Figures 17 and 18.

There is also significant energy left in the scatter of the first backward reflection from shell discontinuities and the scatter of this backward reflected wave generates a secondary scattering pattern in the backscattering fields, as recorded through bistatic measurements and depicted in Figure 22.

Finally, it could be concluded from a comparison of the monostatic data of the damped and the untreated shells, that the damped shell is highly effective in the attenuation of scatter near axial incidence, which is produced by compressional waves propagating in axial direction. This effect is seen in Figure 18.

As mentioned before, the results of the analysis of the data of the damped shell show the effect of internal attachments and slope discontinuities on the scattering behavior very clearly. Further, the results indicate that the measured elastic shell response can be reduced for all observation angles if the shell impedance discontinuities are further reduced. These impedance discontinuities are caused by ring stiffeners, and slope discontinuities between the conical and the cylindrical section of the endcap.

The utilization of a visco-elastic material as the constrained layer proved to be simple in application and effective in the damping process. On the other hand it is clear, that the use of a visco-elastic layer will reduce the hydro-dynamic stiffness of the shell, but this reduction in hydro-dynamic stability can be overcome by an appropriately designed fiber-reinforced damping layer. However, the effect of the radius and orientation of fibers in a constrained layer on the acoustic behavior of internally loaded shells has to be investigated further.

5. References

[1] Ch.N. Corrado, "Mid-Frequency Acoustic Back scattering from Finite Cylindrical Shells and the Influence of Helical Membrane Waves", Ph.D thesis, MIT, Cambridge, MA 1993.

[2] M.C. Junger and D. Feit, *Sound, Structures, and Their Interaction,* (MIT Press, Cambridge, MA 1986).

[3] A.N. Norris and D.A. Rebinsky, "Membrane and Flexural Waves on Thin Shells", Journal of Vibration and Acoustics, Transaction of the ASME, V116 N4, 457-467, (1994).

[4] A.N. Norris, "Rays, Beams, and Quasimodes on Thin Shell Structures", Wave Motion, V21 N2, 127-147, (1992).

[5] A.N. Norris, "Acoustic Coupling to Membrane Waves on Elastic Shells", submitted for publication to JASA, (1993).

[6] A.D. Pierce and H.-G.Kil, "Elastic wave propagation from point excitations of a cylindrical shell", ASME J. Vib. Acoustics, 112, 399-406, (1990).

[7] Y.P. Guo, "Attenuation of Helical Wave Radiation from Cylindrical Shells by Visco-Elastic Layer", Journal of the Acoustical Society of America, 97 (1), 298-308, (1995).

[8] D. Ricks, "Elastodynamic Modeling of Fluid-Loaded Cylindrical Shells with Multiple Layers and Internal Attachments", Ph.D thesis, MIT, Cambridge, MA, 1994.

[9] B.D. Steinberg, *Principles of Aperture and Array System Design*, John Wiley & Sons, New York, 1976.

[10] M. Conti, "Mid-Frequency Acoustic Scattering from Finite Internally-Loaded Cylindrical Shells Near Axial Incidence", Ph.D. thesis, MIT, Cambridge, MA, 1995.

[11] A.C. Ugural, *Stresses in Plates and Shells*, McGraw Hill, 1981.

[12] L. Cremer, M. Heckl, and E.E. Ungar, *Structure Borne Sound*, Springer-Verlag, Berlin, second edition, 1988.

Appendix A. Theoretical Modeling

The presented theoretical study is concerned with vibrations of an infinite, elastic cylindrical shell, which is subjected to fluid-loading on the outside, as a model for a long but finite shell.

A1. Theoretical Analysis

Two theoretical models are discussed in the following; these models were developed by the author and which represent two fundamental answers to the question of how the damping process in cylindrical shells can be modeled. It should be mentioned, that one of these two approaches coincides closely with Guo's modeling of the damping process.

A source of vibration at some point on the cylinder will produce an acoustic field, which will propagate away from the point of contact into the fluid, as well as a variety of waves which will propagate on the shell. Depending on the traveling speed of the waves with regard to the speed of sound in the fluid i.e., if the waves on the shell are subsonic or supersonic, the acoustic energy of these waves will decay exponentially away from the shell or will freely propagate in the fluid. In this analysis only the attenuation of supersonic waves will be shown to be important, because these wave types are responsible for patterns observable in the far field.

A1-1 Theoretical Model

It is known, that the interface of a shell with a relatively heavy fluid medium presents a strongly coupled interactive system, whose dynamic response differs considerably from the behavior of the isolated structure in vacuo. Thus, the forced acoustical response of a three-layer sandwich cylindrical shell with induced fluid loading is formulated as the basis for determining the damping effect of a visco-elastic layer upon the fluid-structure response.

The considered shell structure consists of three isotropic layers with different thicknesses. It is assumed that the three layers are joined together by a perfect bond which enforces the continuity of displacement at the interfaces. The material of the face layers is Nickel and the core material is a visco-elastic material, where tangential shear deformation is taken into account. The analysis of the face layers further employs the Kirchhoff assumptions. The equations of motion are derived on the basis of D'Alemberts Principle. The fluid loading induced by the harmonic forces is computed according to Junger and Feit [2].

The deformations and forces of a three-layer cylindrical shell section are considered as shown in Figure 26. Classical shell theory assumptions are employed for the inner and outer face layers and first-order linear shear deformation is adapted in the tangential components of the core displacements. Note that it is essential in the derivation of the equation of motion, that the thin-shell assumptions are not violated. The classical thin-shell theory is a first-order approximation in the strain quantities under consideration. Therefore the assumptions made are similar to the assumptions made in the Bernoulli-Euler theory for beams. For completeness the classical thin - shell assumptions are given in the following:

- The ratio of shell thickness to radius of curvature of the midsurface is small in comparison with unity, in general this ratio is considerably smaller than 0.1.

- The deflections are small compared with shell thickness.

- Plane sections through a shell taken normal to the midsurface remain plane and become normal to the deformed midsurface, after the shell is subjected to deformation. If a visco-elastic layer is used as the core layer, then this requires the core layer to be fairly stiff in shear - otherwise the above assumptions will be violated.

- The z-direction normal strain, ε_z, is negligible. Stresses and forces in axial and circumferential direction represent integrated quantities over the shell thickness. All geometrical quantities in the definition for forces, force couples, and moments are on the order of magnitude of the shell thickness.

Two cylindrical elastic shells are bonded together with a visco-elastic core material to form a composite structure of mean radius a. The axial, circumferential, and radial displacement components u, v, w and all the forces assumed to act on an infinitesimal part of the shell are shown in Figure 26.

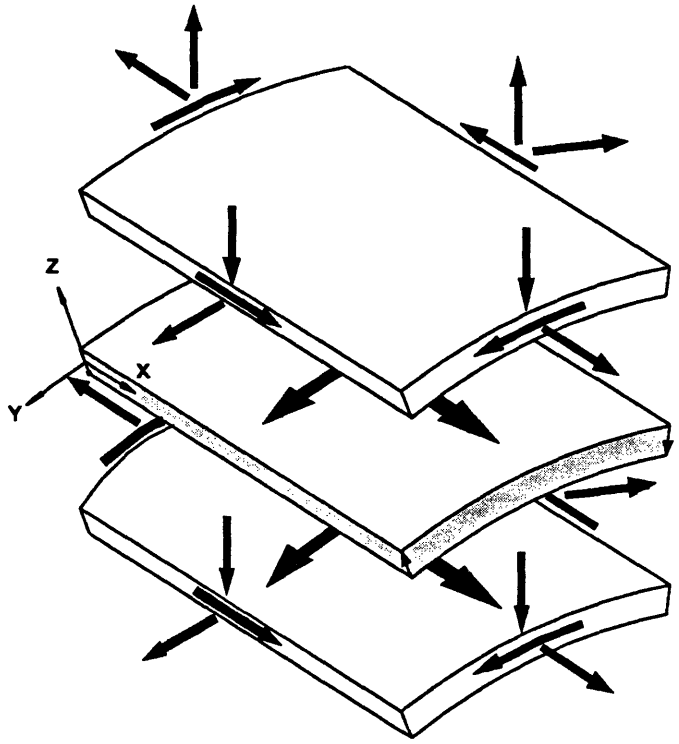

Figure 26. Free body diagram of a differential shell element.

The radial dependence of the normal displacements in the visco-elastic and face layers is neglected. Therefore, based on the assumption that the face layers are bonded together, the following equality will hold:

$$w^o = w^i = w^c$$

with $w = w(x, \phi, t)$ denoting the radial displacement, which remains uniform across the three layers of the shell. The superscripts t, o, i, and c refer to total, outer, inner, and core layers, respectively.

Further, for the model considered herein, it is assumed that u and v is uniform through the thickness for the inner and outer layer. The displacement through the visco-elastic material varies linearly through its thickness and the ratio of shell thickness to radius is sufficiently high so that

the differences in the radii of the layers can be ignored. The Young's modulus, shear modulus, Poisson's ratio, and the thickness of each layer are denoted by E, G, ν, and h, respectively. The axial and circumferential strains ε and the shearing strain γ, in terms of the displacement components [12], are

$$\varepsilon_x^\alpha = \frac{\partial u}{\partial x} - z\frac{\partial^2 w}{\partial x^2}, \qquad \varepsilon_y^\alpha = \frac{\partial v}{R\,\partial\phi} - \frac{w}{R} - \frac{z}{R^2}\frac{\partial^2 w}{\partial\phi^2}, \tag{A.1}$$

$$\gamma_{xy}^\alpha = \frac{1}{R}\frac{\partial u}{\partial\phi} + \frac{\partial v}{\partial x} - \frac{2z}{R}\frac{\partial^2 w}{\partial x\partial\phi}, \qquad \gamma_{yz}^c = \frac{\partial v}{\partial z} + \frac{1}{R}\frac{\partial w}{\partial\phi}, \qquad \gamma_{xz}^c = \frac{\partial u}{\partial z} + \frac{1}{R}\frac{\partial w}{\partial x}, \tag{A.2}$$

where $\alpha = o, i$ and R denotes the shell radius.

From Hooke's law and the strain displacement relations, the stresses can be written in terms of the strains as

$$\sigma_x^\alpha = \frac{E^\alpha}{(1-\nu^2)}(\varepsilon_x^\alpha + \nu\,\varepsilon_y^\alpha), \qquad \sigma_y^\alpha = \frac{E^\alpha}{(1-\nu^2)}(\varepsilon_y^\alpha + \nu\,\varepsilon_x^\alpha), \tag{A.3}$$

$$\tau_{xy}^{\alpha} = G\,\gamma_{xy}^{\alpha}\,,$$
$$\tau_{xz}^{c} = G\,\gamma_{xz}^{c}\,, \qquad \text{(A.4)}$$
$$\tau_{yz}^{c} = G\,\gamma_{yz}^{c}\,,$$

and ν represents the Poisson ratio.

The equation of motion are established by considering circumferential equilibrium of the inner and outer layers and the radial equilibrium of the composite shell element. If the stresses are integrated over the layer thickness along the axial coordinate x and along the azimuthal angle Φ, and all force components of two layers are balanced in three directions, the following equations of motion are obtained,

$$\frac{\partial N_x^o}{\partial x} R\,d\phi dx + \frac{\partial N_{\phi x}^o}{\partial \phi} d\phi dx - N_{xz}^o R\,d\phi dx - p_x^o R d\phi dx = 0\,,$$
$$\frac{\partial N_x^i}{\partial x} R\,d\phi dx + \frac{\partial N_{\phi x}^i}{\partial \phi} d\phi dx + N_{xz}^i R\,d\phi dx - p_x^i R d\phi dx = 0\,,$$
$$\frac{\partial N_\phi^o}{\partial \phi} d\phi dx + \frac{\partial N_{\phi x}^o}{\partial x} R\,d\phi dx - N_{\phi z}^o R\,d\phi dx - Q_\phi^o d\phi dx - p_\phi^o R d\phi dx = 0\,, \qquad \text{(A.5)}$$
$$\frac{\partial N_\phi^i}{\partial \phi} d\phi dx + \frac{\partial N_{\phi x}^i}{\partial x} R\,d\phi dx + N_{\phi z}^i R\,d\phi dx - Q_\phi^i d\phi dx - p_\phi^i R d\phi dx = 0\,,$$
$$\frac{\partial Q_x^i}{\partial x} R\,d\phi dx + \frac{\partial Q_\phi^i}{\partial \phi} d\phi dx + N_\phi^i d\phi dx - b\left(\frac{\partial N_{\phi z}^c}{\partial \phi} + R\frac{\partial N_{xz}^c}{\partial dx}\right) d\phi dx + p_z^i R d\phi dx = 0\,,$$

where $N_{x,\phi,x\phi}$ represents the in-plane normal forces and shear force components of a differential shell element depicted in Figure 26. $Q_{x,\phi}$ represents the radial force component acting on the outside of the shell element. The excitation is purely radial and therefore excitation terms will only appear in the last of the equations in Eq. (A.5).

From Eqs. (A.1) to (A.5), the equations of motion can be written in terms of displacement components as

$$\begin{vmatrix} a_{11} & a_{12} & a_{13} & a_{14} & a_{15} \\ a_{21} & a_{22} & a_{23} & a_{24} & a_{25} \\ a_{31} & a_{32} & a_{33} & a_{34} & a_{35} \\ a_{41} & a_{42} & a_{43} & a_{44} & a_{45} \\ a_{51} & a_{52} & a_{53} & a_{54} & a_{55} \end{vmatrix} \begin{vmatrix} u^o \\ u^i \\ v^o \\ v^i \\ -w \end{vmatrix} = \begin{vmatrix} 0 \\ 0 \\ 0 \\ 0 \\ -(p_i + p_s)\rho^i/cp^{2,m} \end{vmatrix}, \tag{A.6}$$

where

$$a_{11} = h^o \left[\frac{\partial^2}{\partial x^2} + \left(\frac{1-\nu^o}{2R^2}\right)\frac{\partial^2}{\partial \phi^2}\right] - \lambda^o\frac{(1-\nu^c)}{2h^c} + h^o\frac{\omega^2}{cp^{2,o}}, \qquad a_{12} = \lambda^o\frac{(1-\nu^c)}{2h^c},$$

$$a_{13} = h^o\frac{1+\nu^o}{2R}\frac{\partial^2}{\partial\phi\partial x}, \qquad a_{14} = 0,$$

$$a_{15} = \nu^o\frac{h^o}{R}\frac{\partial}{\partial x} - \lambda^o\frac{(1-\nu^c)}{2}\frac{\partial}{\partial x},$$

$$a_{21} = \lambda^i\frac{(1-\nu^c)}{2h^c}, \qquad a_{22} = h^i\left[\frac{\partial^2}{\partial x^2} + \left(\frac{1-\nu^i}{2R^2}\right)\frac{\partial^2}{\partial\phi^2}\right] - \lambda^i\frac{(1-\nu^c)}{2h^c} + h^i\frac{\omega^2}{cp^{2,i}},$$

$$a_{23} = 0, \qquad a_{24} = h^i\frac{1+\nu^i}{2R}\frac{\partial^2}{\partial\phi\partial x},$$

$$a_{25} = \nu^i\frac{h^i}{R}\frac{\partial}{\partial x} - \lambda^i\frac{(1-\nu^c)}{2}\frac{\partial}{\partial x},$$

$$a_{31} = h^o\frac{(1+\nu^o)}{2R}\frac{\partial^2}{\partial x\partial\phi}, \qquad a_{32} = 0,$$

$$a_{33} = h^o\left[\frac{\partial^2}{R^2\partial\phi^2} + \frac{(1-\nu^o)}{2}\frac{\partial^2}{\partial x^2}\right] - \lambda^o\frac{(1-\nu^c)}{2h^c} + h^o\frac{\omega^2}{cp^{2,o}}, \qquad a_{34} = \lambda^o\frac{(1-\nu^c)}{2h^c},$$

$$a_{35} = \frac{h^o}{R^2}\frac{\partial}{\partial\phi} - \lambda^o\frac{(1-\nu^c)}{2}\frac{\partial}{\partial\phi} ,$$

$$a_{41} = 0 , \qquad a_{42} = h^i\frac{(1+\nu^i)}{2R}\frac{\partial^2}{\partial x\partial\phi} ,$$

$$a_{43} = \lambda^i\frac{(1-\nu^c)}{2h^c} , \qquad a_{44} = h^i\left[\frac{\partial^2}{R^2\partial\phi^2} + \frac{(1-\nu^i)}{2}\frac{\partial^2}{\partial x^2}\right] - \lambda^i\frac{(1-\nu^c)}{2h^c} + h^i\frac{\omega^2}{cp^{2,i}} ,$$

$$a_{45} = \frac{h^i}{R^2}\frac{\partial}{\partial\phi} - \lambda^i\frac{(1-\nu^i)}{2}\frac{\partial}{\partial\phi} ,$$

$$a_{51} = \nu^o\frac{h^o}{R}\frac{\partial}{\partial x} - \frac{(1-\nu^c)}{2}\lambda^o R\frac{\partial}{\partial x} ,$$

$$a_{52} = \nu^i\sigma\frac{h^i}{R}\frac{\partial}{\partial x} + \frac{(1-\nu^c)}{2}\lambda^i R\frac{\partial}{\partial x} ,$$

$$a_{53} = \frac{h^o}{R^2}\frac{\partial}{\partial\phi} - \frac{(1-\nu^c)}{2}\lambda^o\frac{\partial}{\partial\phi} ,$$

$$a_{54} = \frac{h^i}{R^2}\sigma\frac{\partial}{\partial\phi} + \frac{(1-\nu^c)}{2}\lambda^i\frac{\partial}{\partial\phi} ,$$

$$a_{55} = (\beta_h^o + \sigma\beta_h^i)\nabla^4 + \frac{(1-\nu^c)}{2}\lambda^o h^c\nabla^2 + \frac{(h^o + \sigma h^i)}{R^2} + \omega^2\left(\frac{h^o}{cp^{2,o}} + \frac{h^i}{cp^{2,m}}\right) ,$$

and

$$cp^{2,\alpha} = \frac{E^\alpha}{\rho^\alpha(1-\nu^{2,\alpha})} ,$$

$$\lambda^\alpha = \frac{E^c}{E^\alpha}\frac{1-\nu^{2,\alpha}}{1-\nu^{2,c}} ,$$

$$\beta_h^\alpha = \frac{h^\alpha}{3}(h^\alpha + 3h^\alpha z + z^2) ,$$

$$cp^{2,m} = \frac{E^o}{\rho^i(1-\nu^{2,o})} ,$$

$$\sigma = \frac{E^i}{E^o}\frac{1-\nu^{2,o}}{1-\nu^{2,i}} .$$

where all symbols represent the quantities as defined in Chapter 2.1.

The equation of motion for this two-layer system will reduce to the well-known, one-layer Donnell-Mushtari equation of motion, if the inner and outer displacement components are added together for a shell, which is symmetric around the midsurface, and if the thickness of the core layer is neglected. The model represented by Eq. (A.6) can predict the damping effect of a soft visco-elastic layer. If the stiffness of the visco-elastic layer is high, then the coupling forces in the visco-elastic layer have to be considered. The shell stresses have to be integrated around the midsurface of the shell cross-section (here $\lambda^a = 0$) and a new system of equations of motion is obtained:

$$\begin{vmatrix} b_{11} & b_{12} & b_{13} & b_{14} & b_{15} \\ b_{21} & b_{22} & b_{23} & b_{24} & b_{25} \\ b_{31} & b_{32} & b_{33} & b_{34} & b_{35} \\ b_{41} & b_{42} & b_{43} & b_{44} & b_{45} \\ b_{51} & b_{52} & b_{53} & b_{54} & b_{55} \end{vmatrix} \begin{vmatrix} u^o \\ u^i \\ v^o \\ v^i \\ -w \end{vmatrix} = \begin{vmatrix} 0 \\ 0 \\ 0 \\ 0 \\ -(p_i+p_s)\rho^i/cp^{2,m} \end{vmatrix} . \qquad \text{(A.7)}$$

The obtained system of equations of motion Eq. (A.7) is similar to system Eq.(A.6), except the following matrix entries:

$$b_{15} = a_{15} + H^o \frac{\partial}{\partial x} \nabla^2 , \qquad b_{25} = a_{25} + H^i \frac{\partial}{\partial x} \nabla^2 ,$$

$$b_{35} = a_{35} + \frac{H^o}{R} \frac{\partial}{\partial \phi} \nabla^2 , \qquad b_{45} = a_{45} + \frac{H^i}{R} \frac{\partial}{\partial \phi} \nabla^2 ,$$

$$b_{51} = a_{51} + H^o \frac{\partial}{\partial x} \nabla^2 , \qquad b_{52} = a_{52} + H^i \sigma \frac{\partial}{\partial x} \nabla^2 ,$$

$$b_{53} = a_{53} + \frac{H^o}{R} \frac{\partial}{\partial \phi} \nabla^2 , \qquad b_{54} = a_{54} + \frac{H^i}{R} \sigma \frac{\partial}{\partial \phi} \nabla^2 ,$$

$$b_{55} = a_{55} + \frac{2}{R} \frac{\partial^2}{\partial x^2} [H^o \nu^o + \sigma H^i \nu^i] + \frac{2}{R^3} \frac{\partial^2}{\partial \phi^2} [H^o + \sigma H^i] ,$$

where

$$H^{\alpha} = \pm\frac{h^{\alpha}(h^{\alpha} + 2z)}{2} .$$

and z represents the radial offset of the lower bounding surface.

The model represented by Eq. (A.7) is based on the assumption of continuity of displacements across the total shell thickness,

$$u^{o} = u^{i} = u^{c}, \qquad v^{o} = v^{i} = v^{c} . \tag{A.8}$$

Eq. (A.7) represents a system with two discrete layers and this model may be used if the core-layer forces in a three-layer system are negligible. In the case of a damped shell with three layers, the approach is the same as shown in Eq. (A.7), but with two additional equations in axial and circumferential direction for the third layer (the equation of motion in the radial direction is only affected by additional h^{c} and H^{c} components at their respective locations in the equation).

If all forces of a three layer shell are considered, Eq. (1) to (3) are obtained. The thin shell results for a constrained layer shell design and shown in the main part of this thesis are based on Eq. (A.7).

A1-2 The Plane Wave Excitation

If the excitation is decomposed into its frequency components, then the traveling waves on the shell have the form $e^{i(kx-\omega t)}$ in complex notation, where k is the wave number and ω is the frequency of the source. The wave number, k, (for each angular order, n) can be determined from the dispersion relation, $D(k,\omega) = 0$. In the solution of the dispersion relation, both real and complex roots can occur, where the complex roots represent acoustic disturbances which decay

away from the source. Therefore, the higher the value for the imaginary part of these complex roots the more the acoustic waves will be damped.

The acoustic response can be obtained by transforming the differential system into an algebraic system utilizing a Fourier transform. Because of the axial symmetry of the shell and radial excitation, the physical quantities of the problem can be decomposed into different angular orders of integer value using a trigonometric transformation in the circumferential direction,

$$\Sigma_{n=-\infty}^{\infty} A_n \cos(n\,\phi)\, e^{ikx}\, e^{i\omega t} \,. \tag{A.9}$$

Now, if a plane wave is used as the excitation source, the acoustic problem can be solved by decomposing the incident plane wave into angular harmonics and using cylindrical wave functions,

$$\begin{aligned} p_i &= P_o\, e^{i(k_x x + k_z z + n\phi)} \\ &= P_o\, e^{ik_x x} \Sigma_{n=0}^{\infty} \epsilon_n\, i^n J_n(k_z z) \cos(n\,\phi) \,, \end{aligned} \tag{A.10}$$

where $\epsilon_n = \begin{cases} 1 & (n = 0) \\ 2 & (n > 0) \end{cases}$ and ϕ is the angle of incidence, measured from the longitudinal shell axis.

The scattering pressure must have a real and imaginary part, representing propagating and decaying waves away from the shell, and it is represented by the Hankel-function of the first kind, $H_n(K_z z) = J_n(k_z z) - iY_n(k_z z)$. Then, the scattering pressure must be of the form,

$$p_s = P_o\, e^{ik_x x} \Sigma_{n=0}^{\infty} C_n\, \epsilon_n\, i^n H_n(k_z z) \cos(n\,\phi) \tag{A.11}$$

with C_n denoting the scattering coefficient. Thus the scattering pressure has the same form as the incident pressure but is modified by the scattering coefficient, which is dependent on each circumferential wave order, n. In addition, for large arguments the Hankel function behaves according to $e^{ik_z z}/\sqrt{ik_z z}$, which equals the mathematical description of a plane wave. The shell

displacement components are expected to have the same form as the incident/scattering pressure,

$$U^{\alpha} = e^{ik_x x} \Sigma_{n=0}^{\infty} U_n^{\alpha} \epsilon_n i^n \cos(n\phi) ,$$
$$V^{\alpha} = e^{ik_x x} \Sigma_{n=0}^{\infty} V_n^{\alpha} \epsilon_n i^n \sin(n\phi) , \qquad (A.12)$$
$$W = e^{ik_x x} \Sigma_{n=0}^{\infty} W_n^{\alpha} \epsilon_n i^n \cos(n\phi) .$$

The time-dependence $e^{i\omega t}$ is suppressed in Eqs. (A.12). The incidence angle, ϕ, is assumed to equal zero, because in this analysis backscattering in the specular direction is studied. In addition to the governing equation of motion the linearized equation of momentum is used to relate the radial surface displacement to the total pressure field,

$$-\frac{\partial p^t}{\partial z} = \rho_{fluid} \frac{\partial^2 w}{\partial t^2} , \qquad (A.13)$$

where $p^t = (p_i + p_s)$. Solving the equation of momentum together with the shell equation of motion, a coupled system with six unknown coefficients is obtained, from which the scattering pressure can be determined.

The plane wave excitation has certain effects on the scattering behavior of the damped shell, which are summarized in the following: The infinite incidence plane wave is propagating with speed of sound through the fluid and can excite only those waves on the infinite cylinder, that are "trace matched". Thus, only supersonic waves on the shell surface will be excited. These supersonic waves can freely radiate away from the shell. Compressional and shear waves are supersonic, and therefore, these wave types will mainly contribute to the far-field backscattering pressure. The speed of bending waves depends upon the frequency of excitation, and only very high frequencies will result in supersonic bending waves; in this case, however, the governing equation of motion will not produce adequate results - because then the assumption that the wave length is larger then the thickness of the shell can not be considered to be true anymore.

In the analysis of pressure fields it is customary to introduce a so-called form function. It quantifies the far-field scattering pressure as a function of frequency ka, aspect angle θ, and azimuthal angle ϕ. The normalized form function can be written as,

$$\begin{aligned} |f_\infty| &= \left| \frac{p_s}{p_i} \right| \sqrt{\frac{2z}{a}} \\ &= \frac{2}{\sqrt{\pi k_z a}} \left| \Sigma_{n=0}^{\infty} \epsilon_n C_n \cos(n\phi) \right| . \end{aligned} \tag{A.14}$$

As mentioned in Section 3.2 the measurements were conducted in the near-field of the shell. A frequency dependent correction factors for the far-field target strength has to be applied to compensate for the near-field effects in the measurements. It was computed by using a line array model [1]. The line model used consisted of 57 equally spaced transducers separated by a distance of 0.0148 m. The spacing was chosen such that $d < \lambda/2$ over the frequency range of interest. 51 sources located in the center of the line array were uniformly tapered and 3 sources on each end were hanning tapered to represent decreased scattering contribution of the endcaps. The total pressure field is computed by integrating over the pressure contribution of all transducers. The pressure contribution of a single transducer [9] is written as,

$$dp = A\, T(z)\, \frac{e^{ikl}}{l}\, dz, \tag{A.15}$$

where

$$\begin{aligned} l &= r \sqrt{1 + \frac{2z}{r}\sin\theta + \frac{z^2}{r^2}} \\ &= r \left(1 + \frac{z}{r}\sin\theta + \frac{z^2}{2r^2}\cos^2\theta + \ldots\right) . \end{aligned} \tag{A.16}$$

Retaining the second order term in Eq. (A.16) and integrating over the entire array length the pressures for a radius of 2 m and a radius of 50 m was obtained. These pressures were used to calculate the target strength correction factors as

$$T_{corr}(\omega) = 20 \log \left(\left| \frac{p(\omega, r = 50)}{p(\omega, r = 2)} \right| \right) + 20 \log \left(\frac{50}{2}\right) . \qquad (A.17)$$

It is noted that the correction factors are the same for all shell measurement data, because all the measurements were recorded with the same experimental configuration. The frequency dependent correction factors are shown in Figure 27. The averaged value of this correction factor is 8.2 dB (averaged over $2 < ka < 12$).

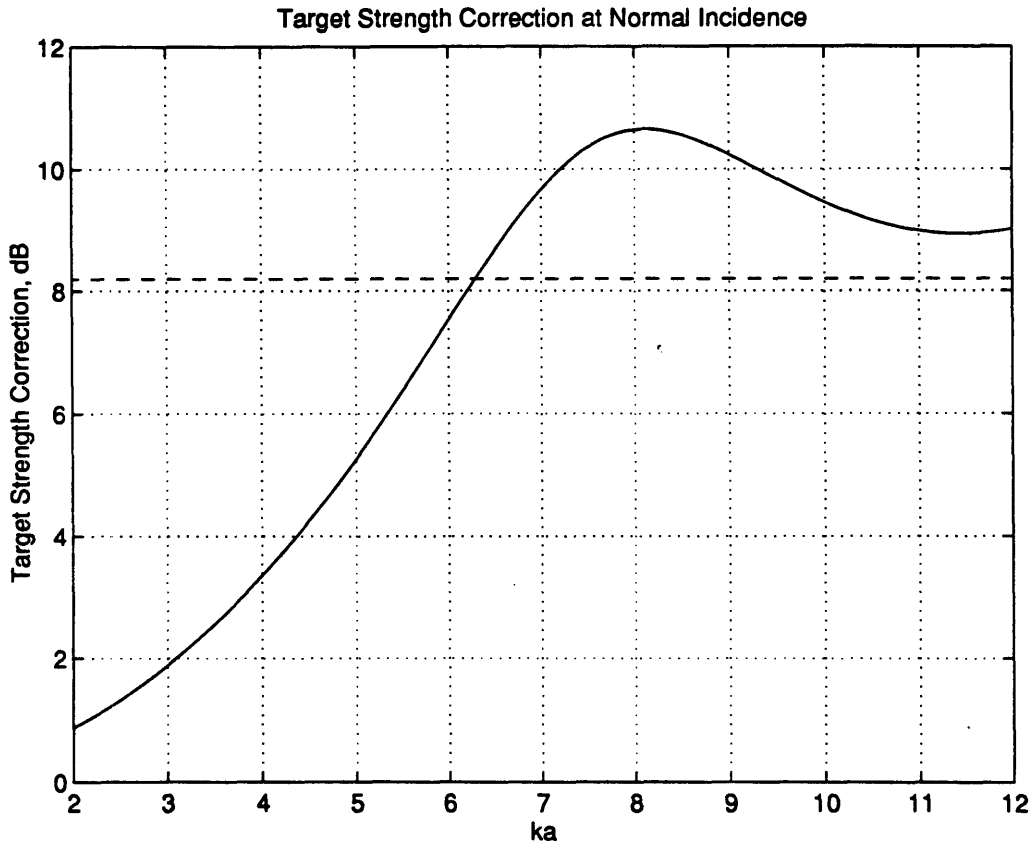

Figure 27. Target strength correction for near-field measurements.

A1-3 Damping of a Cylindrical Shell

Damping is very often a quite complicated process in mechanical structures. Nevertheless, it was shown previously [1,2,7,10,12], that the complicated process of damping can be modeled by introducing a complex material constant. In this analysis the Young's modulus is assumed to be of the form,

$$E^* = E_R - i\,\eta E_I\,. \tag{A.21}$$

Then the compressional wave speed is given by

$$c_p^* = \sqrt{\frac{E_{Re} - i\,\eta E_{Im}}{\rho}}\,, \tag{A.22}$$

or in a first approximation,

$$c_p^* \approx \sqrt{\frac{E_{Re}}{\rho}} - i\,\frac{\eta}{2}\sqrt{\left(\frac{E_{Im}}{\rho}\right)^{-1}} = c_{P,Re} - i\,\eta c_{p,Im}\,. \tag{A.23}$$

As can be seen from Eq. (A.23), the compressional speed, c_p^*, is complex and as a consequence the wave number, $k^* = \omega/c_p^*$, becomes a complex quantity. For a wave traveling in axial direction, x, with time dependence, $e^{i\omega t}$, the wave can be characterized by

$$e^{i\,(k_x x + \omega t)}\,. \tag{A.24}$$

Substituting the complex wave number, k^*, in axial direction, $k_x^* = k^* \cos\theta$, into Eq. (A.24), the damped wave traveling in axial direction can be found to be

$$e^{-(k_{x,Im}\,x)}\,e^{i\,[k_{x,Re}\,x + \omega t]}\,. \tag{A.25}$$

The damped wave is characterized by an envelope, which shows a decay with the spatial coordinate, x. It is noted, that the displacement components are averaged across the thickness in the classical theory of thin-shells. Therefore the model, represented by Eq. (A.6), also considers the averaged displacement component of each layer across its respective thickness. The same displacement distribution across the shell thickness can be expected if a soft visco-elastic layer is applied in a composite shell design under plane wave excitation.

It is expected that in a real-life scenario, there is no considerable difference in the averaged inner and outer displacement components - but it is also expected, that an *absolute* displacement distribution will exist, which may deviate from the averaged displacement magnitude for each layer.

Appendix B. Experimental Configuration

In the experimental testing of the visco-elastically damped shell the configuration shown in Figure 28 was used.

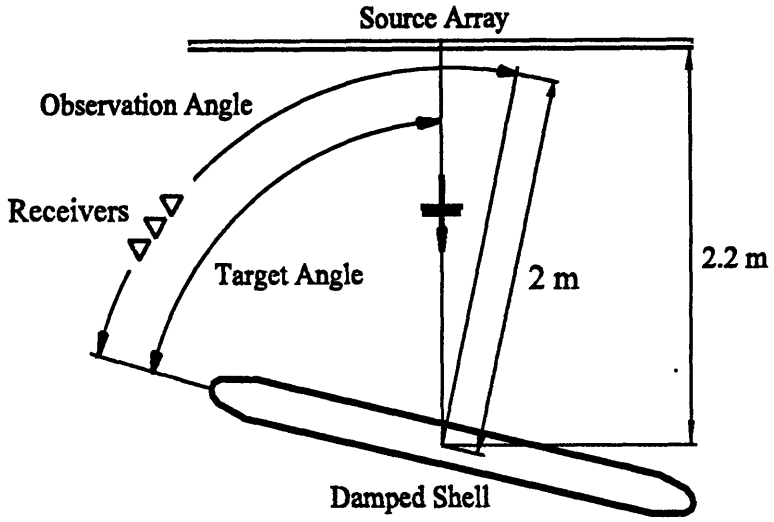

Figure 28. Experimental configuration during testing of NRL-model 5100 (damped shell).

The model tested was insonified by a gaussian pulse with a time duration of 50 microseconds. It produced a flat frequency spectrum over the frequency range of 2<ka<10. Reference source signal strength measurements were conducted, which allowed deconvolution of the measurement data. The target center was located approximately 2.2 m away from the source array. The shell was rotated in the plane of the source array in one degree increments over a range of angles from 0 degrees to 90 degrees for bistatic measurements and 0 degrees to 360 degrees for monostatic measurements. The receivers were located in a circle with a radius of 2m measured from the target (shell) center, as shown in Figure 24. Testing configurations for the untreated shells and additional detailabout testing procedures and the utilized data acquisition system can be found in Reference [1].